NPS-57Zi71121A

NAVAL POSTGRADUATE SCHOOL

Monterey, California

ELECTROHYDRODYNAMICS (EHD)

RESEARCH

by

O. Biblarz

SCAR

10 December 1971

65p.

NAVAL POSTGRADUATE SCHOOL
Monterey, California

Rear Admiral A. S. Goodfellow
Superintendent

M. U. Clauser
Provost

ABSTRACT:

This is the third year-end report on the EHD contract.

Work with the steam injector continued during the past year. The definition of the slip parameter for unsteady flow has been used in conjunction with velocity profiles measured with a hot wire anemometer to evaluate the potential role of EHD (or EGD) in anemometry. A direct measurement of particle size (using holographic interferometry) indicated that there are no particles of size 10^{-4} m or greater. A computer program describing the EHD flow has been written.

FOREWORD

This is a continuation of the EHD Research program started on September of 1968 at the Naval Postgraduate School, Monterey, California. This work was sponsored by the Naval Air Systems Command under the technical cognizance of Dr. H. R. Rosenwasser.

One Master thesis was generated and it is included in the Appendix. A paper entitled "Unsteady-Flow Electrogasdynamics" is presently being submitted for publication. A Navy patent has been applied for the spectral anemometry principle. A progress paper was given at the Energy Conversion Colloquium held during 9-10 November at the Naval Postgraduate School.

The help of LCDR Bohley and Mr. Patrick Hickey is gratefully acknowledged. The laser holographic measurements were made possible through the assistance and cooperation of Professor Collins of the Aeronautics Department, NPS.

TABLE OF CONTENTS

LIST OF FIGURES (Main Text)

LIST OF SYMBOLS (Main Text)

E_b = Breakdown field strength

$|E|$ = Absolute value of the electric field

R = Particle radius

$S(\omega)$ = Slip parameter of frequency ω

$V(\omega)$ = RMS velocity at frequency ω

μ = Mobility of particles

τ_v = Equilibration time for particles

ω = Frequency

I. INTRODUCTION

During the past year progress was made basically along three fronts: First, the anemometry application was the subject of an MS thesis (included here as the Appendix). Also, a paper tying-in the work on anemometry and the EHD generator was written and is presently being submitted for publication. Next, an attempt was made at measuring particle size directly (i.e., by laser holography). Last, a computer program which solves the combined Laplace-Poisson equations inside the generator was written and checked-out.

This report includes the final hot-wire anemometer frequency profile of the region being investigated. As pointed out in last year's report[1], these measurements were made along the centerline in the wake of the cylinder at a location 5mm downstream of the exit plane of the injector nozzle. A review of the optimum frequency response concepts follows the hot wire data. Also included are a discussion of the laser-holograms and a brief summary of the computer program.

II. HOT-WIRE ANEMOMETER READINGS

The unit that gave the final results reported here is a Thermo Systems, Inc. model 1051-2 constant temperature hot wire, with a frequency response of 50 KHz.

The hot wire readings were to be used as a standard of comparison for the EGD data but because the hot wire calibration is not appropriate for two phase flows, air was substituted for the steam in the cylinder[1]. The air flow was matched so as to give the same momentum as the steam.

The absence of droplets extended the life of the hot wires which was very marginal to begin with due to the intense vorticity of the wake of the cylinder. Another complication arose from the fact that the air flow through the steam nozzle was typically as a different temperature from the main air flowing around the cylinder. Several attempts were made at equalizing the two temperatures. The most reliable data seemed to indicate that the nozzle flow does not have a measurable effect on the main flow. This holds for distances of at least 5mm away from the nozzle exit plane. The resulting profile is shown in Figure 1. It represents the main air and the nozzle air (8 psig) but it is indistinguishable from the hot wire profile for the main air itself. There are two dominant frequencies apparent from this figure, namely, 1.2 KHz and 10 KHz. The first one represents twice the Strouhal frequency for the cylinder and is appropriately so because the measurements were taken along the centerline of the wake where the vortices, shed off the cylinder on alternating sides, add up. The Reynolds number based on cylinder diameter for this flow (55 m/sec) is 8×10^4 so that the boundary layer on the cylinder is laminar. The second important frequency apparent from Figure 1 seems to be associated with the nozzle that injects steam into the wake, see Figure 2. The 10 KHz peak appeared whether or not there was air issuing from the nozzle. The exit diameter of this nozzle is about 2mm which is some ten times smaller than the cylinder diameter and perhaps appropriately the frequency is nearly 10 times higher. It was observed further that 10 KHz is apparently a high enough frequency so that the dissipation of the vortices is high; at a station

10mm away from the nozzle exit plane, the 10 KHz peak disappears whereas the 1.2 KHz peak remains nearly as intense. So the fluid viscosity can act on these "lesser whorls" but the flow is still to be considered pseudo-turbulent since the vortices at the Strouhal frequency are basically two dimensional.

There are no other significant contributions to the vorticity because the flow turbulence is carefully removed upstream and all measurements are made away from the wall boundary layers. There is one uncertainty that remains, however, and that involves whether or not the presence of large particles (i.e., two-phase flow) shifts the intense part of the profile towards the lower frequencies. The larger particles can absorb some of the eddy energy more or less continuously at this may cause a significant shift. This could be described with a different "effective" viscosity for the two-phase flow. The only way to resolve this dilema is to make measurements with either a laser or an ultrasonic anemometer. The laser device relies on the presence of large particles and measures their Doppler shift. The accuracy of these devices is considered below that of the hot wire at the present.

III. OPTIMUM FREQUENCY RESPONSE

It has been pointed out[1] that in the anemometer application of the EGD probe the charged particle size determines the frequency response of the device. This is clear insofar as the inertia of the particle governs how fast it can equilibrate with the eddies.

In last year's report, it was shown that the slip parameter (S) for unsteady flow could be written as

$$S_{max} = \frac{\mu E_b}{V(\omega)} + \tau_v \omega \qquad (1)$$

where ω = frequency

μ = particle mobility

E_b = breakdown field strength

$V(\omega)$ = RMS intensity of the free stream velocity at the frequency ω

τ_v = equilibration time for the particles

Since the mass of the particle only appears in τ_v, the question arises as to what may be a desired criterion for the frequency response as a function of size which si consistent with a small slip parameter. This criterion may be arbitrary, i.e., fixing $\omega\tau_v$ to be some small fraction. Figure 3 shows a plot of ω vs radius for values of $\omega\tau_v$ equal to 10^{-2} and 10^{-3}. This choice fixes ω without regard to the value of the first term in Equation 1 which in itself may be higher than 10^{-2}; however, a high slip due to a high mobility is undesirable for either the generator or the anemometer. Note further that if $V(\omega)$ is very small i.e., close to zero, then the slip may be very high but since there is no significant contribution by the flow at this frequency the slip value is unimportant.

Since the slip parameter plays a significant role in the generator efficiency, it is necessary to determine the spectral distribution of the flow inside the generator and calculate the slip at each of the dominant frequencies.

IV. LASER HOLOGRAPHY

In last year's Final Report[1], results from charge distribution measurements seem to indicate the existence of charged droplets of size of about 100 μ m. This is because about 3×10^8 electrons per pulse had been measured at a steam pressure of 13 psig. The resolution that we could obtain with the laser apparatus was itself about 100 μm and the limiting factor[2,3] was the graininess of the hologram reproduced object. As can be seen from Figures 4 and 5, no particles can be detected and we conclude that the particles are of a size much smaller than 100 μm. Note that the nozzle exit diameter is 0.14 inches or 2.5 mm.

Other work in last year's Final Report seem to indicate that sizes were in the order of 10 μm and less. The direct measurement of these particles is a the limit of the technique even with a refined set-up.

V. COMPUTER PROGRAM

As shown by Minardi[4] the potential distribution within an EGD channel is described by a "combined Laplace-Poisson" equation. The two equations are required by the two-phase space charge nature of the EGD environment. Poisson's equation models the space-charge region, while Laplace's equation models the space-charge free region. Electrode geometry and space-charge effects on the potential distribution are of interest in the design of EGD devices. The solution of the governing equations will show these effects. However, a closed-form

solution is often very difficult to find, and any attempts at a solution will be complicated by the varying boundary conditions imposed by the electrodes.

In order to have an analytical input to the design process, a numerical solution method (successive over-relaxation) was programmed for the IBM 360 computer system. Finite difference equations, derived from a Taylor-series expansion about the point in question, were used to build the numerical model. The program has the capability for solving axisymmetric and two-dimensional channel flows. The program output is designed to give both numerical and graphical representations of the solution.

Of importance in the computer modeling of the EGD device is the fluid dynamics involved. By means of a similar program, Minardi[5] has shown that for particle sizes of interest, the fluid dynamics may be uncoupled from the electrodynamics. Thus it is possible to limit modeling of the dielectric gas flow to a constant rate of jet expansion and insure conservation of charge within the jet.

Input variables to the program typically include those describing the electrode geometry, dielectric characteristics, charged particle characteristics, flow control, variables matrix dimensions and the output desired. The program simulates a steady state picture of the entire EGD situation by the superposition of two separate matrices. One matrix will carry all potential information, while the other matrix carries both charge distribution and some flow control information. The initial part of the program is devoted to setting up these matrices.

Once this has been accomplished, the program calls for an iterative calculation to determine the potential distribution, and a calculation for the $|E|$ -field distribution. Remainder of the program is devoted to output of these results.

The program was applied to the geometry shown in Figure 2. The dielectric gas used was steam issuing at 397 m/sec from the nozzle. This corresponds to a reservoir conditions of 8 psig and 240°F. This is a slightly super-heated steam. Particle charging was considered to be corona limited, giving a particle mobility of 1×10^{-7} m^2/v-sec. A dielectric constant of 8.9×10^{-12} coul/v-m is used. Attractor potential was 3 KV, and the collector potential was 50 volts below ground. Figure 6 is the plotted output of the potential distribution, showing lines of constant potential. Figure 7 is the plotted output of $|E|$ - field distribution, showing lines of constant value of E. The potential has been normalized with respect to attractor or corona potential, and the E-field values with respect to the breakdown field of 3×10^6 v/m. The geometry is represented by the cross-hatched points.

VI. CONCLUSIONS AND RECOMMENDATIONS

It is evident from the results shown in the Appendix that we have been able to achieve "acceptable" responses from the EGD probe up to 1000 Hz. This acceptability is based on the correctness of the hot-wire data used for comparison. From Figure 3, this implies that particle sizes are centered about 1 μm or higher radii. From the holographic measurements, we know the particles are not much above

10 μm. Our efforts at changing the superheat of the steam in order to affect particle size have indicated that this is not the only relevant parameter; apparently what happens to the charged particles outisde of the nozzle is equally important. There, of course, the behavior is somewhat random and a statistical sample is needed. Lowering the pressure from 13 psig to 8 psig is a step in the right direction but apparently something happens that gives multiple peaks in the distribution of particles. These results point out two things: First, better humidity control and some dilution of the steam inside the cylinder (through, say, a bleed of nitrogen) may be needed to achieve a reduction of particle size. Second, the present response is sufficient to measure some interesting turbulent flows which need not be as complicated as the wake of the cylinder (for example, grid-generated turbulence).

The computer study will be directed toward the design of guard-electrodes inside the generator channel which will improve the output of the device. The program is further useful in pointing out regions of high electric field. This is quite significant for any EHD power generator.

The definition of the coupling of the charged particles with an unsteady flow field remains as an important goal of this project. Most EHD flows are unsteady to some extent and a low slip parameter for steady flow may not be good enough if significant velocity components exist at non-zero frequencies.

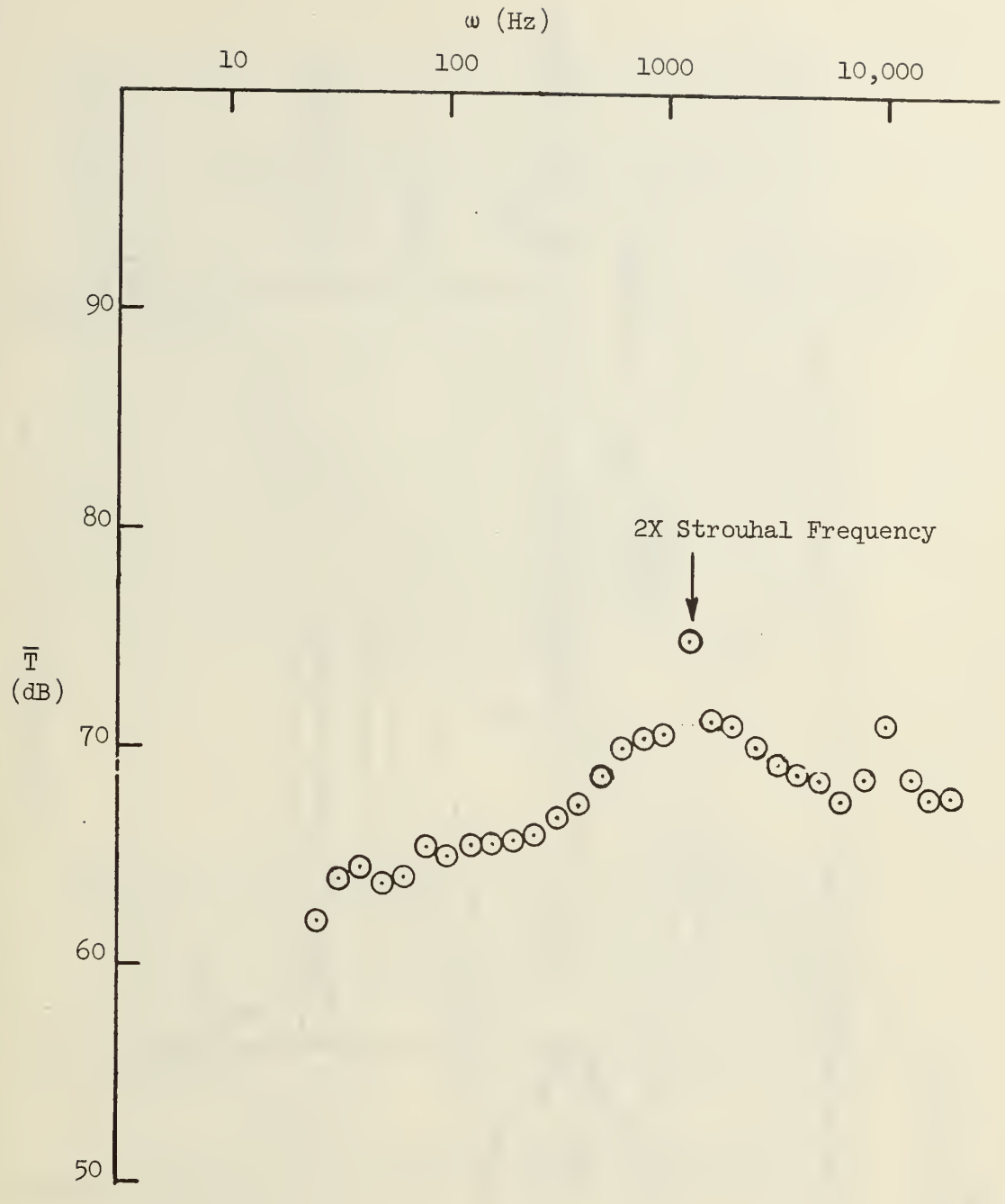

FIGURE 1. COMPOSITE OF HOT-WIRE ANEMOMETER DATA

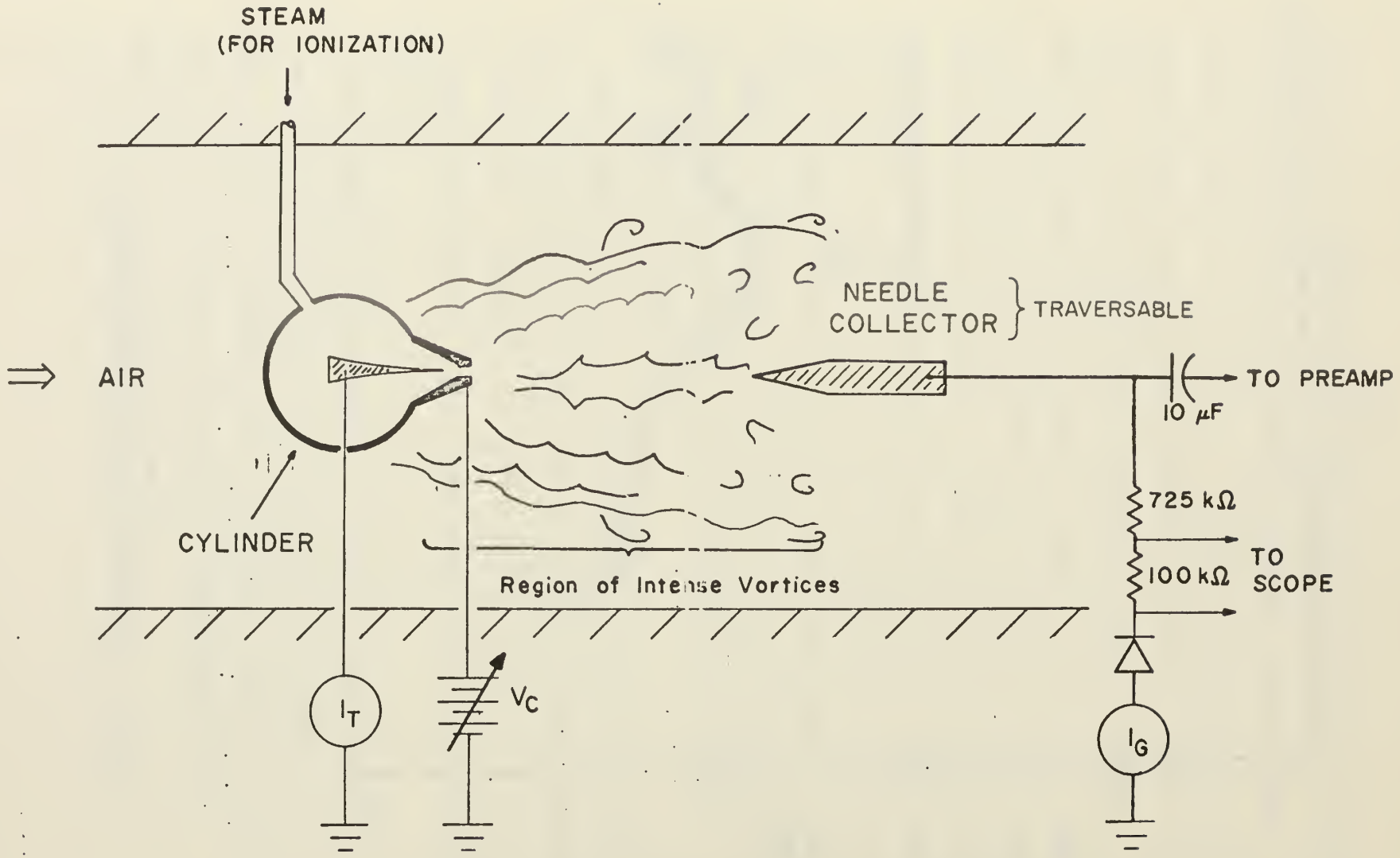

FIGURE 2 EGD GENERATOR SCHEMATIC

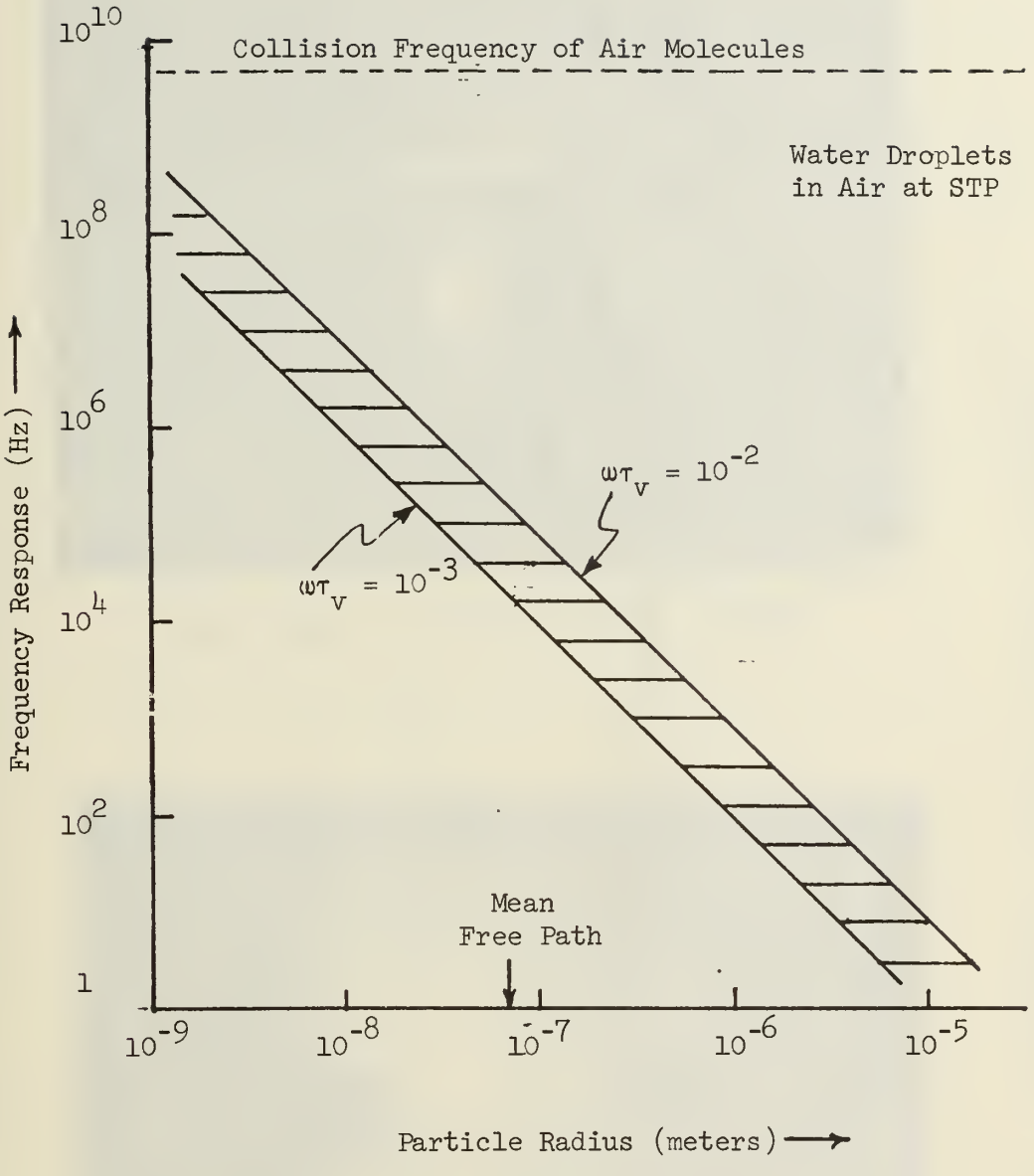

FIGURE 3 OPTIMUM FREQUENCY RESPONSE
AS A FUNCTION OF THE RADIUS

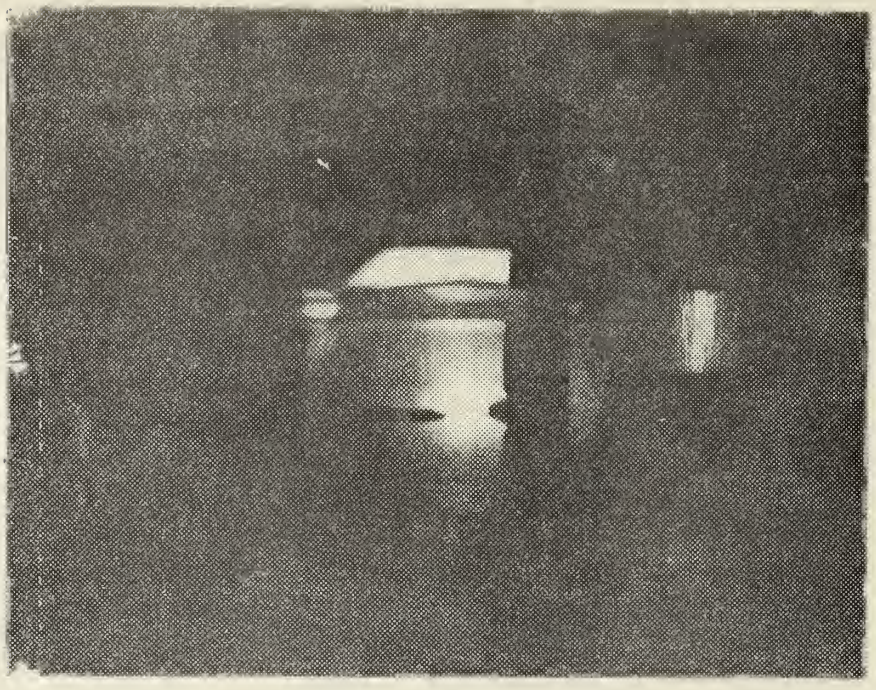

FIGURE 4 LASER HOLOGRAM OF VIRTUAL IMAGE

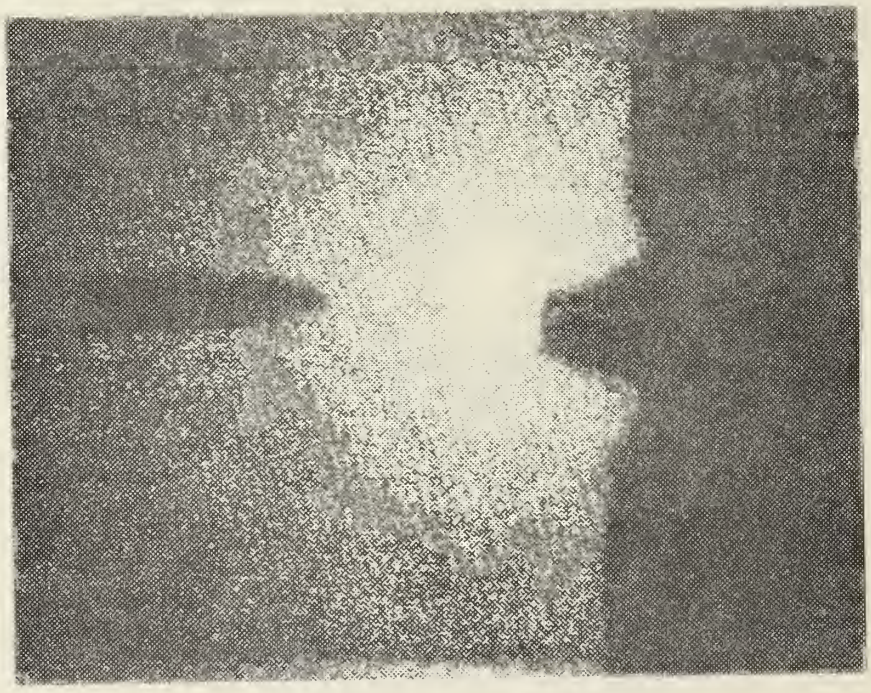

FIGURE 5 ENLARGED VIEW OF TEST SECTION

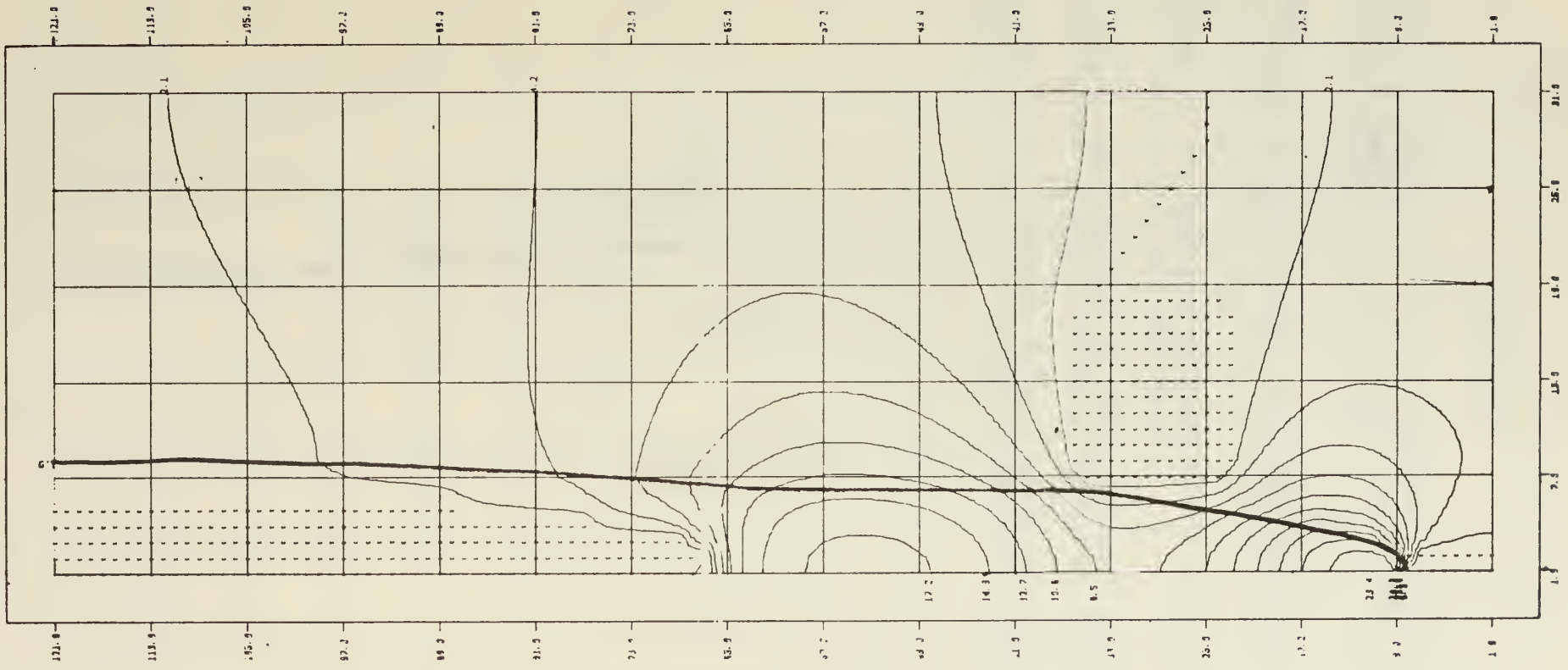

FIGURE 6 TWO DIMENSIONAL OUTPUT OF POTENTIAL DISTRIBUTION

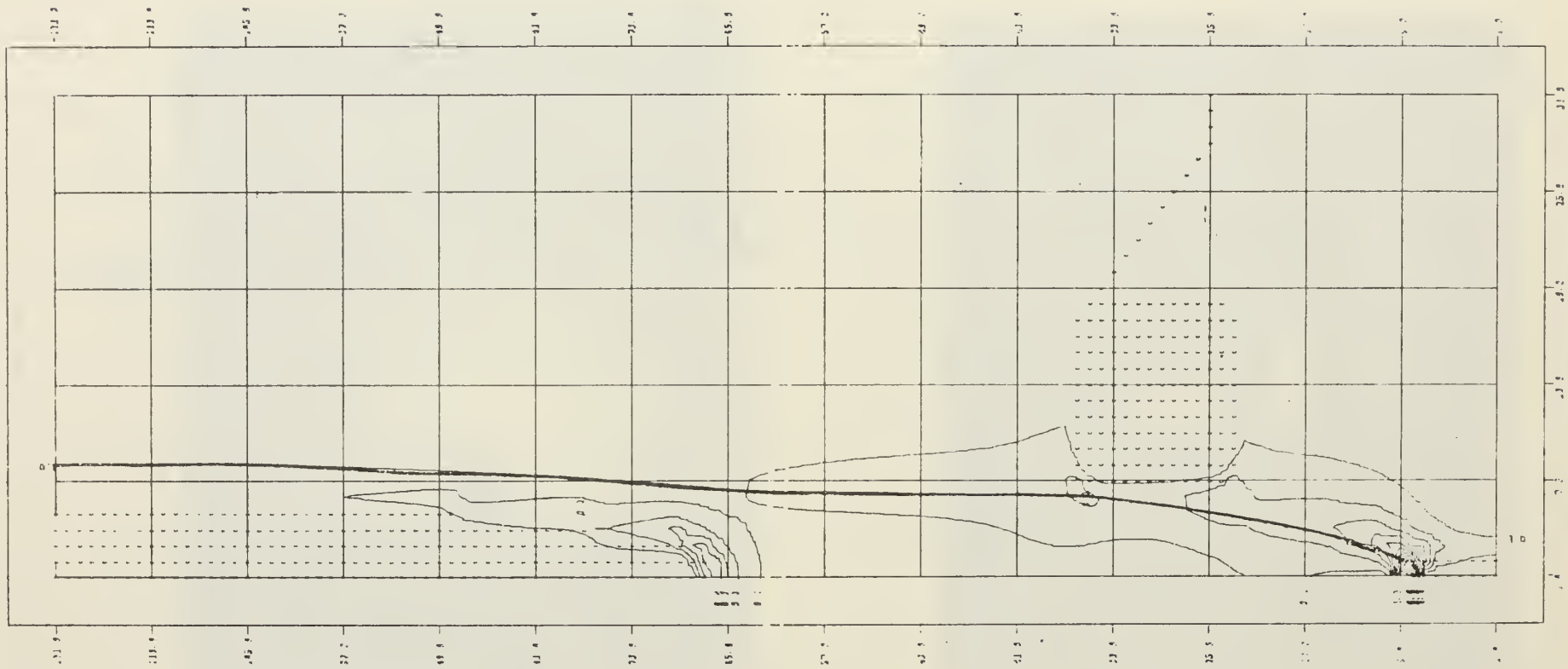

FIGURE 7 TWO-DIMENSIONAL OUTPUT DISTRIBUTION OF THE ELECTRIC FIELD

REFERENCES

1. Biblarz, O., Woehler, K. P., and Gawain, T. H., "EHD Research - Final Report for the Year 1969-70", Naval Postgraduate School Report, NPS-57ZI0121A, Dec. 1970.

2. Mathews, B. J., Wuerker, R. E., and Harrje, B. T., "Small Droplet Measuring Technique", Tech. Rep. AFRPL-TR-68-156, July 1968 (Air Force Rocket Prop. Law, Edwards AFB).

3. Wuerker, R. E., "Research on Electrostatic Charged Droplet Streams", ARL 67-0211, Oct 1967 (TRW Report).

4. Lawson, M. and Wattendorf, F. (Eds), "Selected Topics in Electrofluiddynamic Energy Conversion," AGARograph 122, Dec. 1968.

5. Minardi, J. E., "Computer Program for the Calculation of Electric Fields in an Electrofluiddynamic Generator", Report ARL 68-0156, Aug. 1968.

United States
Naval Postgraduate School

THESIS

SPECTRAL ANEMOMETRY

WITH AN ELECTROGASDYNAMIC PROBE

by

Ronald John Laib

Thesis Advisor: O. Biblarz

September 1971

ABSTRACT

This study involves the measurement of RMS velocities covering the frequency spectrum 25 to 20,000 hertz using an electrogasdynamic (EGD) probe. Previous work proved the feasibility of this investigation. The flow of air behind a circular cylinder was measured. The freestream velocity was 185 ft/sec. Charged water droplets entering the wake through a jet in the cylinder at sonic velocity acted as the media for conveying information to the probe. Hot-wire anemometer readings made in the same spectral range were used as the standard of comparison. However, these need further refinement.

Small droplet formation was optimized by determination and control of the relative humidity of the freestream, steam temperature and steam pressure. Optimum droplet charge was then determined and controlled with corona voltage. A 10 to 15 decibel increase in high frequency response and stable performance resulted.

TABLE OF CONTENTS

LIST OF ILLUSTRATIONS

TABLE OF SYMBOLS AND ABBREVIATIONS

A	amperes
AC	alternating current
C	Celsius (Centigrade)
cm	centimeter
C	centerline
D	diameter
dB	decibels
E	electric field strength (volts/meter)
E_b	breakdown electric field strength (volts/meter)
EGD	electrogasdynamic
f	frequency (Hertz)
F	farad, Fahrenheit
fps	feet per second
ft	feet
GR	General Radio
Hz	Hertz (cycles/second)
I_C	corona current (microamperes)
I_G	generator collector probe current (microamperes)
I_T	total current, needle current (microamperes)
j	current density (amperes per square meters)
kHz	kilohertz
kV	kilovolts
kΩ	kilohms
L	distance between collector probe and corona ring (mm)
lb_m	pound mass

m	meter
mm	millimeter
P	pressure (pounds per square inch)
psia	pounds per square inch absolute
psig	pounds per square inch gage
R	resistance (ohms)
RH	relative humidity (percent)
RMS	root-mean-square
s	slip (defined as $\mu E/U_\infty$ and dimensionless)
SAT	saturation
sec	seconds
T	temperature (degrees Fahrenheit)
T_{SAT}	saturation temperature (degrees Fahrenheit)
TSI	Thermal Systems, Inc. Hot-wire anemometer
$\overline{T}$	intensity of turbulence (dB)
$\overline{T}_E$	turbulence intensity as measured with EGD probe (dB)
$\overline{T}_h$	turbulence intensity as measured with hot-wire (dB)
$\overline{T}_{max}$	maximum turbulence intensity occuring in the frequency spectrum, usually at the Strouhal or twice the Strouhal frequency
$\overline{T}_{min}$	minimum turbulence intensity occuring in the frequency spectrum, usually at 20 kHz, the highest frequency sampled
U_∞	freestream velocity ahead of the cylinder (fps)
V	volt
V_C	corona voltage, potential difference between needle and attractor ring (volts)
V_{RMS}	root-mean-square voltage (dB)
Vdc	direct current voltage

X	x-axis on X-Y display in 30 discrete frequencies from 25 to 20,000 Hz
Y	y-axis on X-Y display indicating signal intensity from 40 to 120 dB
$\Delta\overline{T}$	comparison of measured turbulence intensity between hot-wire data and EGD data (dB)
$\Delta\overline{T}_{HFR}$	a measure of the high frequency response by comparing the turbulence intensity at a high frequency (usually at 20kHz) to the most intense turbulence in the frequency spectrum (dB)
μ	mobility (square meters per volt-seconds)
μA	microamperes
μF	microfarad
ρ_e	charge density (coulomb per cubic meter)
Ω	ohms
ω	circular frequency, $2\pi f$ (radians per second)
~	approximately
°	degree
"	inches
>	greater than
#	number
%	percent

I. INTRODUCTION

Previous work in Electrogasdynamics has indicated a definite correlation between EGD probe readings of collector current and the mean and rms velocities measured by a hot-wire anemometer in the turbulent wake of a circular cylinder [6]. This thesis is an attempt to improve the spectral correspondence of EGD probe measurements to hot-wire results. The probe is a stainless steel rod with a sharpened tip which is placed in a moving stream of air where it collects charged particles. For charged particles of proper size and charge, sufficient coupling may result in the turbulent flow to allow measurement of the spectrum of turbulence intensity.

The advantages of the EGD probe as a diagnostic tool over the hot-wire anemometer are manifold. The probe is very rugged, allowing probing of intense turbulent fields. It is very simple and inexpensive and, therefore, can be easily manufactured. The probe tip area is small and symmetrical, allowing better spatial resolution than the hot-wire. Since the very small charged particles can react to high frequency oscillations, the frequency response of the EGD probe may be higher than that of the hot-wire. In addition, signals from the EGD probe, which are electrical in nature, need little or no further amplification [7]. Effects corresponding to the thermal inertia of hot-wires are not present. There is no requirement to feed the

output through a linearizer since the EGD output is already linear, i.e., a direct measurement. Also eliminated is the effect that free convection currents have on the hot-wire zero setting. In the case of two-phase fluids, the EGD probe needs no separate calibration and will withstand the impact of charged droplets or particles whereas the fragile hot-wire will readily break under these conditions. The main disadvantages of the EGD mechanism are the requirements for a source of charged particles of optimum size and charge and for a high voltage supply (along with the necessary safety precautions). The optima appear to be rather critical.

The specific objectives of this thesis are: 1) improvement of the high frequency response of the EGD probe [5]; 2) the elimination or explanation of inconsistencies between the EGD results and the hot-wire results; and 3) the determination of the effect that various parameters, i.e., humidity, steam pressure and temperature, the ratio of collector current to total current, etc, have on the results. A lesser objective was finding a means of facilitating the reduction of data for comparison to hot-wire data.

This work complements part of a comprehensive, long-term project being conducted by Assistant Professor Oscar Biblarz, Department of Aeronautics, Naval Postgraduate School. Existing EGD equipment installed in Building 230 at the Naval Postgraduate School was utilized.

II. THEORY

In 1959 Bennett [2] pointed out that by carrying electrical charge in the volume of a stream of air instead of on the surface of a belt, a gaseous Van de Graff generator could be built. Since a greater volume of charge would be carried at higher speeds, much higher current should result. This marked the beginning of the EGD generator.

The basic EGD mechanism involves particles which are introduced into an air stream or other suitable gas at the entrance of the test section (Figure 1). For the source of charges an aerosol flow in conjunction with an ionizer are used. Saturated steam is injected through a corona discharge into the "turbulent" wake of a cylinder. The corona discharge is produced by applying a high voltage between a sharp needle and an attractor ring which is embedded in the wall of the steam nozzle located on the downstream side of a right circular cylinder. Electrons from the negative needle drift toward the attractor and attach themselves to the then-growing water droplets forming negative charged particles. Some of these charged particles are in turn dragged or convected by the air flow down the conversion channel where their electrons are transferred to a metallic collector probe. Since the collector is also negatively charged, work is accomplished and some of the kinetic energy of the gas has been changed directly into electrical energy. These charges flow

through an outside circuit and return to the needle. If the energy drained from the gas is minimal, then the flow has not been disturbed by the conversion process.

One of the important parameters here is particle size. If the particle is too small, i.e., very mobile, the drift velocity of the particles becomes large and current loss results as exemplified in the current density equation for EGD,

$$\vec{j} = \rho_e (\vec{U}_\infty - \vec{\mu E}) \qquad (1)$$

where μE is the drift velocity. By rearranging the equation in its scalar, one-dimensional form one obtains

$$j = \rho_e \left(1 - \frac{\mu E}{U_\infty}\right) U_\infty \qquad (2)$$

and slip can be defined as

$$s = \frac{\mu E}{U_\infty} . \qquad (3)$$

For a certain range of radii, as the charged particle size decreases, the mobility constant increases (Figure 2) and hence slip increases [3,9].

Mobility is a function of mass and charge of the particle. Since the ability of a charged particle to follow the turbulent eddies in the cylinder wake is a function of its mass, an increase in size results in lower frequency response of the charged particle. This can be seen by considering the effects of inertia in a moving particle. A particle with less mass can accelerate, decelerate, and change direction much faster than a particle of greater mass exposed to the same forces.

One of the problems in previous investigation [6] has been the generation of steam droplets of correct size for high-frequency coupling and correct charge for low mobility. Injection of particles ranging between 10^{-6} to 10^{-7} meters charged in a corona field results in a maximum drift velocity of one to ten meters per second but allows particles to fluctuate with frequencies up to 50 kHz [4]. Previous work showed a high frequency drop for the EGD probe in comparison with hot-wire anemometer measurements [6]. An analysis indicated that the particle radius was on the order of five microns [4]. Therefore it seems that the size of the steam droplets can be reduced by decreasing the condensation which should, in turn, result in an increase in EGD probe bandwidth. Previous work showed that "condensation" was decreased by lowering the steam pressure to below 8.3 psig [4]. Wetness could be decreased by superheating the steam as it travels from the steam generator to the cylinder exit nozzle. In addition, Reference 13 (unpublished) and some of our preliminary work indicated that certain ranges of relative humidity of air in the channel could enhance particle size after injection into the air flow. Thus, high-frequency response could also be enhanced by controlling relative humidity.

One last area concerns the standard of comparison. The hot-wire anemometer measures the turbulence in a single-phase flow while the EDG probe measures a two-phase

flow. The frequency spectrum of these two flows may differ since the droplets most likely enhance the low frequency spectrum.

III. EQUIPMENT

The heart of the apparatus is the small plexiglass wind tunnel test section. The inside dimensions are two by four inches in cross section and ten inches in length. The test section contains a steam injector unit which is fed by a heated steam line from a steam generator [10]. The aerosol injector nozzle consists of a stainless steel ring embedded in the cylinder wall which allows the injection of condensing steam into the turbulent wake of the cylinder (Figure 3).

The steel ring also serves as the corona ring positive electrode of the aerosol ionizer. The negative electrode consists of a steel needle positioned on the corona ring centerline but slightly recessed. A Sorensen High-Voltage DC Power Supply provides the high potential between the ring and needle necessary to negatively charge the steam particles as they pass through the throat of the nozzle (at sonic velocity) into the turbulent cylinder wake. The potential difference is monitored by a Sensitive Research electrostatic voltmeter. A few millimeters downstream from the cylinder nozzle a third electrode, consisting of a stainless steel probe with a rounded tip (Figure 4), collects the current and thereby detects the frequency spectrum of the turbulent wake via the information carried by the charged particles.

The air is supplied by a Carrier three-stage centrifugal compressor with a maximum flow rate of 4000 cubic

feet per minute and a maximum pressure ratio of two. This air is fed through a cooling bank into the main plenum which is attached to the plexiglass test section. The valve on the cooling bank which controls the amount of air being cooled also enables control of the temperature and hence the relative humidity of the air (Figure 5). The air passes through the test section and around the cylinder, then mixes with the steam jet. The particles are convected to the collector probe, where they are neutralized, and the water-air mixture flows out of the test section into the atmosphere.

The current from the collector probe is fed into a black box which houses the circuitry for the probe (Figure 6). The three International Rectifier diodes prevent reverse current flow [11]. A Simpson microammeter measures the collector current. The capacitor and the neon bulb safety switch protect the frequency analyzer. The capacitance is selected large enough to ensure a phase shift of less than one degree in the frequency spectrum from 25 hertz to 20 kilohertz and to accomodate the high voltages which are present (Appendix A).

The pre-amplifier (Figure 7) is a self-powered unit consisting of a UA741C operational amplifier, resistors, and a battery. It provides a gain of ten over a frequency range of 100 kilohertz. A shunt resistance of 39,000 ohms is placed across the input in order to avoid saturating the operational amplifier in the preamplifier, i.e., one third of the signal is bled off by this shunt.

The frequency analyzer is a General Radio Company Type 1921 Real Time Analyzer (Figure 8). This consists of a 1925 Multifilter and a 1926 Multichannel RMS Detector. The signal (Figure 9) from the preamplifier is put into the multifilter, separated according to frequency, put into the RMS detector where the data are converted to binary digital form and the rms level computed by true linear integration. The computed data are then displayed digitally on the rms detector nixie-tubes and the analog form of the data is projected graphically on a Hewett-Packard X-Y display. Either a Tektronix Type RM 15 or a Type 551 Dual Beam oscilloscope is used to monitor the signal input to the frequency analyzer.

The hot-wire data of this experiment were collected with a Thermo Systems, Incorporated, Model 1050 and 1051-D, constant temperature hot-wire anemometer (Figure 10). The frequency response of the TSI equipment was superior to the frequency response of two other constant temperature hot-wire anemometers which were also tried, i.e., a Flow Corporation Constant Temperature Anemometer, Model 900, and a Security Associates, Model 100, hot-wire anemometer. In addition, the TSI unit had a built-in signal generator that enabled simplified procedures for frequency calibration. A Kronhite Model 3202R bandpass filter was used in conjunction with the TSI unit to filter out the noise from outside the test frequency spectrum, which was 25 to 20,000 hertz.

Other equipment included a psychrometer for measuring test section air humidity, a Simpson microammeter for measuring needle current and a voltage regulator for regulating line voltage.

IV. PROCEDURES

The experimental procedure developed from an initial familiarization with the operation of the apparatus and a desire to start with a verification of previous work. This produced results similar to those reported in Reference 6.

The succeeding runs involved a change from a 0.5 microfarad, 2000 Vdc capacitor to a 10 microfarad, 2000 Vdc capacitor in order to eliminate a phase shift in the portion of the spectrum below 250 hertz (Appendix A). A closer correspondence in the lower half of the frequency spectrum now existed, between the EGD turbulence intensity ($\overline{T}_E$) and the hot-wire turbulence intensity ($\overline{T}_h$), than measured in previous work [6].

Asbestos insulation was wrapped around the bare portion of copper tubing immediately below the cylinder. This prevented early cooling, and subsequent condensation, from forming particles of too large a mass, which translates to a great inertia and a low mobility. During the test runs to check these changes, attention was given primarily to tape heat (this tape heats the line between the steam generator and the cylinder in the air stream), steam pressure, and applied voltage. The temperature range was between 230°F and 288°F, the pressure between 7.9 to 14.1 psig, and the voltage between 215 to 3.1 kilovolts.

Since much of the data taken on different days showed little correlation even when the above parameters remained

unchanged, it was necessary to investigate other parameters. Closer observation of the relative humidity, use of a more accurate device for measurement of humidity, and measurement of humidity in the test section during operation revealed that the best results occurred on days when the relative humidity in the channel was less than 46%.

For operation at 25% relative humidity, test section temperature ranged between 95°F to 125°F. Difficulty was encountered in getting values of collector current and total current greater than zero when the relative humidity was 25%. Even at 30%, I_G and I_T tended to be erratic, the microammeters registering zero approximately half of the time. Good results occurred at 32% and this value was chosen for subsequent testing.

The next portion of the experiment was devoted to a thorough testing of the equipment after it was discovered that the internal calibration voltage was occasionally erratic. The General Radio equipment tested in accordance with manual specifications. Noise in the output at the low frequencies (most prevalent around 60 hertz) was reduced by grounding all equipment used in the experiment. A line voltage regulator was installed to decrease fluctuations in line voltage which might affect the equipment and results.

A method of comparing existing hot-wire results with EGD measurements was devised using the multifilter unit. By subtracting out the values (in decibels) of the turbulence

intensity as measured by a hot-wire throughout the frequency spectrum on each of the multifilter channels, any deviation from a straight line on the X-Y display gave an immediate indication of the portion of the spectrum with which the EGD measurements did not favorably compare and the amount by which the intensity differed from the hot-wire data. Because it appeared that some values of the multifilter settings would subtract out a greater value of turbulence intensity than current EGD measurements were producing, the preamplifier was incorporated.

The hot-wire anemometer portion of this experiment was conducted to obtain measurements of turbulence intensity, $\overline{T}_h$, at a nozzle pressure of eight psig and to verify previous data taken at 13 psig. In order to simulate the jet effects but avoid the two-phase flow in which the hot-wire calibration is not useful and also to avoid breaking the hot-wires by droplet impact, the steam unit was disconnected and air at the same pressure was injected into the cylinder and out of the nozzle at 8 and 13 psig [10]. A limited amount of testing (which occurred before the failure of a field-effect transistor) with the Security Associates Hot-Wire Anemometer produced results which agreed with those of reference [6].

A Thermo Systems, Incorporated (TSI) constant temperature anemometer provided a much greater intensity at the high frequency end of the spectrum than had been previously measured (Figures 11 and 12), especially when nozzle air

was on. Figure 11 was the result obtained using a DISA 55F31 probe. All succeeding runs were made with probes used in previous work which are locally manufactured. Subsequent runs with a bandpass filter did not improve the results. It was later discovered, however, that a signal greater than 0.5 volts was possibly injected into the General Radio 1560-P40 preamplifier, damaging the field-effect transistor. Even though hot-wire measurements were made bypassing this preamplifier, it did obtain power from the frequency analyzer and was left connected to the analyzer. It is not known whether this could have caused a stray signal to be injected into the analyzer causing this unexpected, high frequency "tail." Another measurement with the TSI unit was attempted after the above experience and culminated in failure to the TSI unit before any results could be obtained.

The final portion of this experiment produced the EGD results reported herein. A smaller stainless steel probe (0.062 inch diameter) replaced the 0.125 inch steel probe used initially [6]. It was felt that a smaller probe would sample a more localized area and not tend to average the turbulent eddies present in a larger volume of space. A new preamplifier (Figure 7) replaced the General Radio 1560-40. A shunt resistance was incorporated to avoid over-driving the operational amplifier. Channel humidity was held at 32%, as measured at the exit of the test section, eight centimeters aft of the cylinder nozzle. Tape

temperatures were varied between 230°F and 295°F. Generator collector current was varied between zero and 10.2 microamperes and applied voltage between zero and 4.43 kilovolts. Collector currents less than 0.2 microamperes were not measured.

The frequency analyzer converted the AC electrical input from AC voltage to the appropriate value in decibels. The measure of turbulence intensity, $\overline{T}$, at each frequency sampled, was expressed in dB and read directly from the X-Y display or the nixie tubes (Appendix B). The procedure developed for comparing the EGD data with the hot-wire results is as follows: $\overline{T}_E$ represents the value of turbulence intensity measured with the EGD probe as given by the frequency analyzer and expressed in decibels. $\overline{T}_h$ is likewise the value of turbulence intensity measured with the hot-wire anemometer. If the difference, $\Delta\overline{T} = \overline{T}_h - \overline{T}_E$, is the same (± 1 dB for error) for each frequency, then the difference results solely from the difference in amplification of the two signals and the two signals are considered to be identical. In this context $\overline{T} = \log_{10} T'_g(f)$ (Appendix C).

The procedure developed for determining the high frequency response involved a comparison of the difference in intensity between the most turbulent and the least turbulent frequencies. $\overline{T}_{max}$ is the maximum turbulence intensity, usually found at either the Strouhal or twice the Strouhal frequency. $\overline{T}_{min}$ is the minimum turbulence intensity, in

decibels, normally found at the highest frequency. $\Delta\overline{T}_{HFR} = \overline{T}_{max} - \overline{T}_{min}$ is a measure of the difference in intensity of the turbulence between the two frequencies. If this difference is small, then a good relative high frequency response is indicated. $\Delta\overline{T}_{HFR}$ will always have a value greater than zero since, theoretically, turbulent vertices at high frequencies dissociate rapidly to lower frequency vertices [7]. The typical intensity versus frequency curve for a free jet exhibits a gradual decrease in intensity as the frequency increases [7]. The best (smallest) value of $\Delta\overline{T}_{HFR}$ obtained for both EGD and hot-wire data was 12 dB.

V. RESULTS AND DISCUSSION

Good results were consistently obtained when little or no tape heat was applied and when the collector current was very carefully controlled (Table I). Figure 13 shows a corresponding drop in high frequency response as temperature is increased. In order to examine and compare data, a plot of pressure versus density for various values of temperature (Figure 14) was constructed from steam tables [1,8]. This graph was used to convert values of pressure and temperature into corresponding values of density. A check of the steam pressure and temperature values imposed during the experiment, on this plot, reveals that best results were obtained when points lay in the saturated or supersaturated regions.

Two methods of comparing EGD and hot-wire data were used, both using the data shown in Figure 11 as the standard of comparison. Figures 15 through 17 show typical results at 12 to 13 psig with varying temperatures and voltages. With the tape heat turned off, the temperature of the steam at this pressure is 240°F. Saturation temperatures of the steam for these pressures are 244°F and 246°F respectively. Figures 18 through 20 show typical results at 8 psig at various temperatures and voltages. At this pressure the saturation temperature is 235°F and the steam temperature with the tape heat off is 230°F. These results are compared with the best hot-wire anemometer

data available. These data were chosen as the standard of comparison since these were the first data collected with the TSI unit and are expected to be free from any effects due to subsequent malfunctioning electronics. Since all data are already converted to decibels, to ratio (see Appendix C) the desired points one simply takes the difference of the logarithm of the plotted points at each frequency, measured from some arbitrary reference line, to the points to be matched. Twice the Strouhal frequency was chosen as a reference point since it is the most dominant point on the EGD and hot-wire data collected and also since the frequencies just beyond this point are most responsive to changes in parameters.

The second method of comparing EGD data with hot-wire data was by inserting the hot-wire data into the multi-filter as explained earlier. Figures 21 and 22 show a comparison of typical results displayed during testing.

Figure 23 shows the effect of the density of the steam on the current efficiency (I_G/I_T) for the two-phase fluid. In addition to the sensitivity of the current efficiency to a small change in voltage, the effect of an increase in density is to require a higher voltage in order to obtain the same current efficiency. This shifting of the curves to the right is similar to that reported by Whitby [12] for the effect of pressure (temperature was held constant) in a single-phase fluid (air).

Comparisons of Table I with Figure 13 and Figures 15 through 22 reveal that the best high frequency response, i.e., when $\Delta\overline{T}_{HFR}$ is least, generally occurs when the steam temperature is at or below saturation temperature for a given pressure. Figure 24 is a plot of pressure versus high frequency response for three ranges of temperature to saturation temperature ratios. The relative humidity and the collector probe distance remained constant. The corona voltage was held constant at three kilovolts with exceptions shown beside the data points. The best high frequency response (lowest $\Delta\overline{T}_{HFR}$) occurs at the super-saturation and saturation temperatures with the best results in the eight psig pressure range.

Figure 25 shows that a definite optimum voltage exists for operation at good high-frequency response. All other variables are held constant but a slight decrease in the relative humidity from 34% to 32% and a slight increase in pressure from 8.1 to 8.2 psig during the experiment may have had an effect on the optimum collector current and on the current efficiency. The accompanying changes in collector current and current efficiency are shown. After a "triggering" voltage is attained, collector current increases linearly until finally a plateau is reached. The graph shows that the optimum current efficiency does not occur at the optimum voltage, although some previous observations indicated that good results occurred at a current efficiency of 0.2 to 0.5 and at a higher collector

current. Figure 26 shows the effect of current efficiency for three different temperatures with other parameters held constant.

VI. CONCLUSIONS

It is concluded that an electrogasdynamic probe can indeed by successfully used to measure intense turbulent fields. Results comparable to or better than some of the existing hot-wire anemonmeters have been obtained.

The following specific conclusions are drawn:

1. A controlled relative humidity of 32% resulted in a significant improvement in the measurement of turbulence intensity in the high frequency range of the spectrum.

2. Little or no tape heat gave optimum results (Figure 22). This parameter is a highly critical one. A change of 1°F can, at times, make a difference of measuring a highly intense turbulence or not detecting any turbulence at 20 kHz. Sometimes saturation temperature provides optimum results. At other times no tape heat (5°F below saturation temperature) provides optimum results. Even in this last case, an increase in tape heat of one degree results in a marked steadiness of total current and collector current. An increase of an additional 1°F would steady the current even more but, for some runs, would also result in a significant high frequency detection loss. This fact is contrary to expectation, (earlier investigation indicated that the steam droplets seemed too large already).

3. A ratio of collector current to total current greater than 0.20 seemed to provide best results (Figure 26).

4. A marked improvement could sometimes be seen during transient conditions, especially after a change in voltage.

The time required to reach steady state conditions is generally 30 seconds to one minute. However, in a few instances, transients were noted even after five minutes, indicating that steady state conditions are important.

5. An optimum applied voltage range exists, below which no collector current is produced and above which no high frequency turbulence can be measured. This latter phenonemon may be due to an increasing charge built up per particle, resulting in an increased drift velocity back upstream to the attractor ring (Figure 25).

6. The effect of an increase in steam pressure is to shift the current efficiency curves to the right (Figure 23). This is comparable to conclusions drawn by Whitby [10] for single-phase flow. Saturation effects of the steam were lost in converting pressure and temperature to density, however, and are not accounted for in this figure. These also seem to play an important role.

7. Eight psig seems better than thirteen psig. This is in agreement with our previous arguments for smaller mass particles.

8. Total collected current seemed to have an effect. For best results a collector current of one-half microampere or greater was required (Table I).

VII. RECOMMENDATIONS

Several areas need to be further explored in order to refine the electrogasdynamic probe and enhance future applications of this device. The areas are the following:

1. Measurement of the turbulence intensity with state-of-the-art hot-wire anemometer equipment to determine an accurate and consistent turbulence intensity frequency spectrum.

2. An investigation into the effect of higher applied voltages on the production of charged particles and a better high voltage supply, i.e., regulated to avoid ± 60 volt fluctuations at 3.0 kilovolts (RMS ripple factor is 2.0%).

3. Better instrumentation for the control of steam pressure and temperature, i.e., more accurate monitoring of these data. Temperature control should be within at least ± 0.5°F, preferably ± 0.2°F and pressure control to at least ± 0.05 psi. This would allow accurate determination of steady state conditions and insure that the critical parameters are indeed constant. Also, continuous monitoring of air humidity upstream of the cylinder is desirable to eliminate interruption of the experiment for humidity measurement and to preclude any unknown changes from occurring between measurements.

4. A study to determine whether there is any significant difference between the turbulent field of a single-phase fluid and that of the fluid when a second phase is introduced. It is possible that the two-phase flow may shift the spectrum towards lower frequencies by virtue of the large, massive particles which are present.

5. Elimination of the temperature difference between the free stream and the nozzle air. In addition to the lack of two-phase flow, using the hot-wire as a reference introduces another discrepancy - the presence of two temperatures in the fluid. Since the hot-wire measures temperature, any sensing of intermittent temperatures due to two different temperatures rather than to a difference in turbulence intensity could lead to a significant distortion of the frequency spectrum curve.

6. A theoretical study of the nature and frequency range of the turbulence in the wake of the cylinder and nozzle to determine if, indeed, the hot-wire anemometer is measuring all effects present.

7. Further investigation of the effect of small changes in temperature and pressure on the formation of droplets and the production of collector current at various frequency ranges in the turbulence spectrum. An accurate determination of the size of the droplets as a function of the various parameters, especially temperature and ppressure, at a given humidity, will greatly aid in determinimg the proper environment for the future use of the EGD probe.

DATE	RH	P	T	V_C	I_G	I_G/I_T	$\Delta\overline{T}_{HFR}$	REMARKS
Oct. 7	~46%	12.0 psig	240°F	2.5 kV	<0.5μA	<0.25	30 dB	
14	~80	12.4	230	2.65	0	0	47	
21	~70	12.5	249	2.85	0.5	0.09	23	
27	~32	12.3	242	3.0	1.5	0.3	18	
Nov. 18	65	14.1	250	2.6	0.2	0.04	~43	
30	50	12.8	240	2.8	0.2	0.05	24	
Jan. 12	32	13.2	242	2.75	0.4	0.11	~33	
Feb. 12	31	12.0	240	2.8	0.6	0.17	18	Discharge Occasionally Erratic
May 12	29	8.1	230	2.9	0.4	0.11	21	I_G, I_T = 0 @ RH = 25%
28	31	8.0	230	2.9	0	0	18	
June 1	32	7.8	245	3.2	2.5	0.25	12	Least Intensity @ 4000 Hz
2	32	8.1	255	3.0	1.0	0.29	29	
3	33	8.1	230	3.0	0.4	0.09	15	
3	31	8.0	245	3.0	0.8	0.18	14	Parameters Not Stabilized
4	35	8.0	245	2.85	0.9	0.36	27	
7	32	13.0	242	4.4	7.0	0.38	27	
21	32	8.1	234	2.67	1.0	0.67	17	Good Results Near Sat. Temp.
30	32	8.0	231	2.98	0.9	0.23	12	$\Delta\overline{T}_{HFR}$ = 0 @ T > 232°F

TABLE I. Summary of Best EGD Results (L = 5 mm)

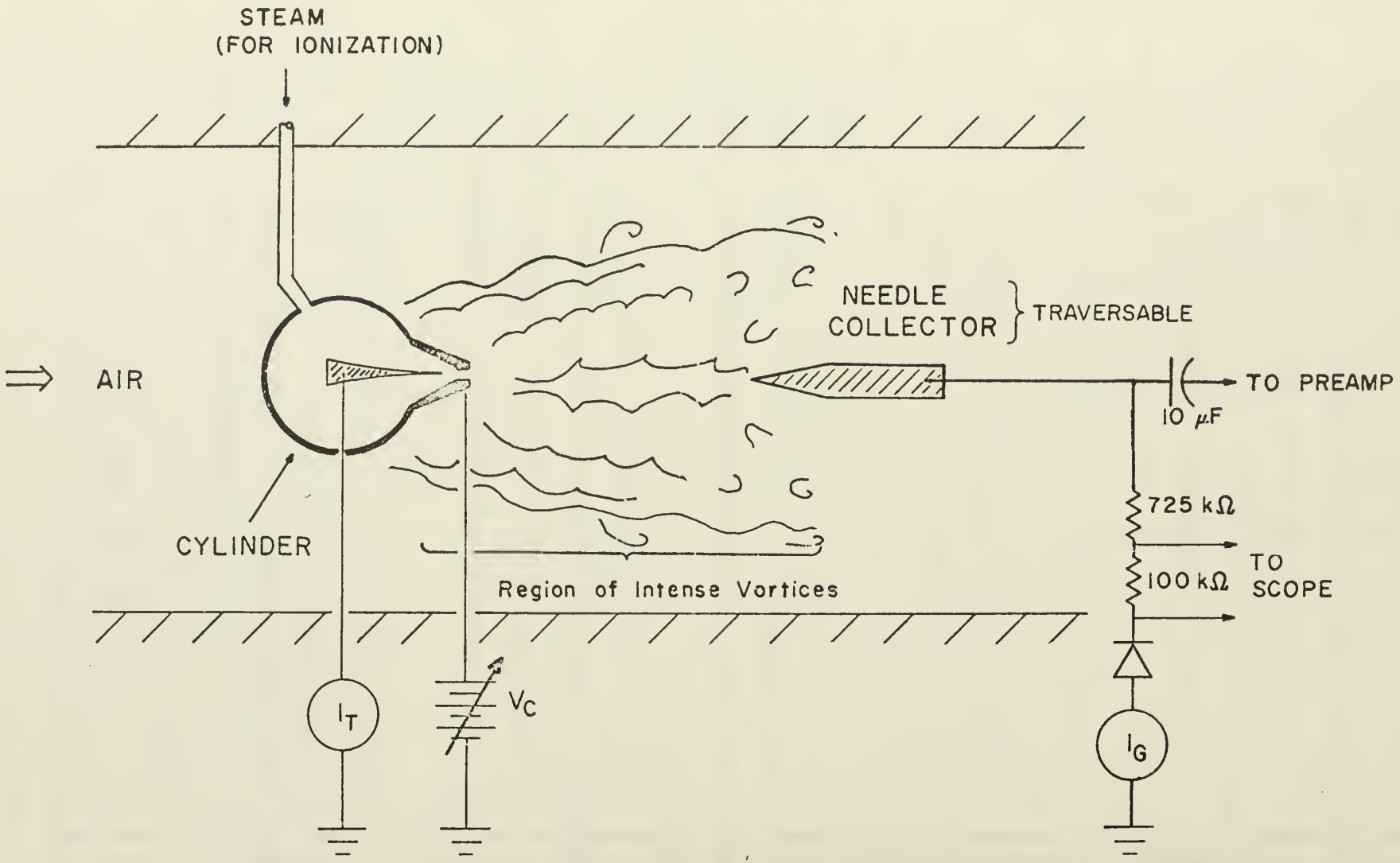

FIGURE I. EGD GENERATOR SCHEMATIC

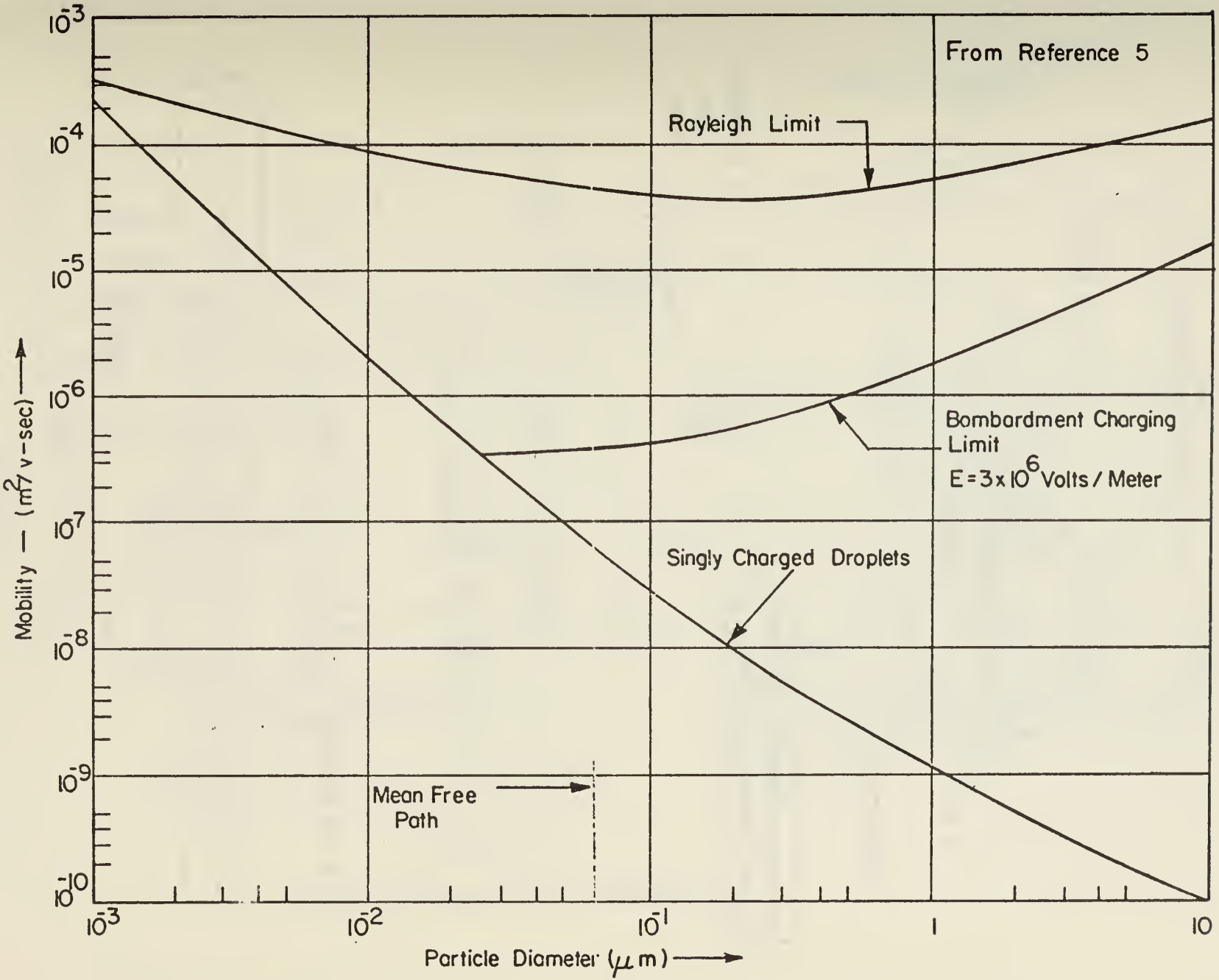

FIGURE 2. MOBILITY OF WATER DROPLETS IN AIR AT 1-ATM. AND 20°C

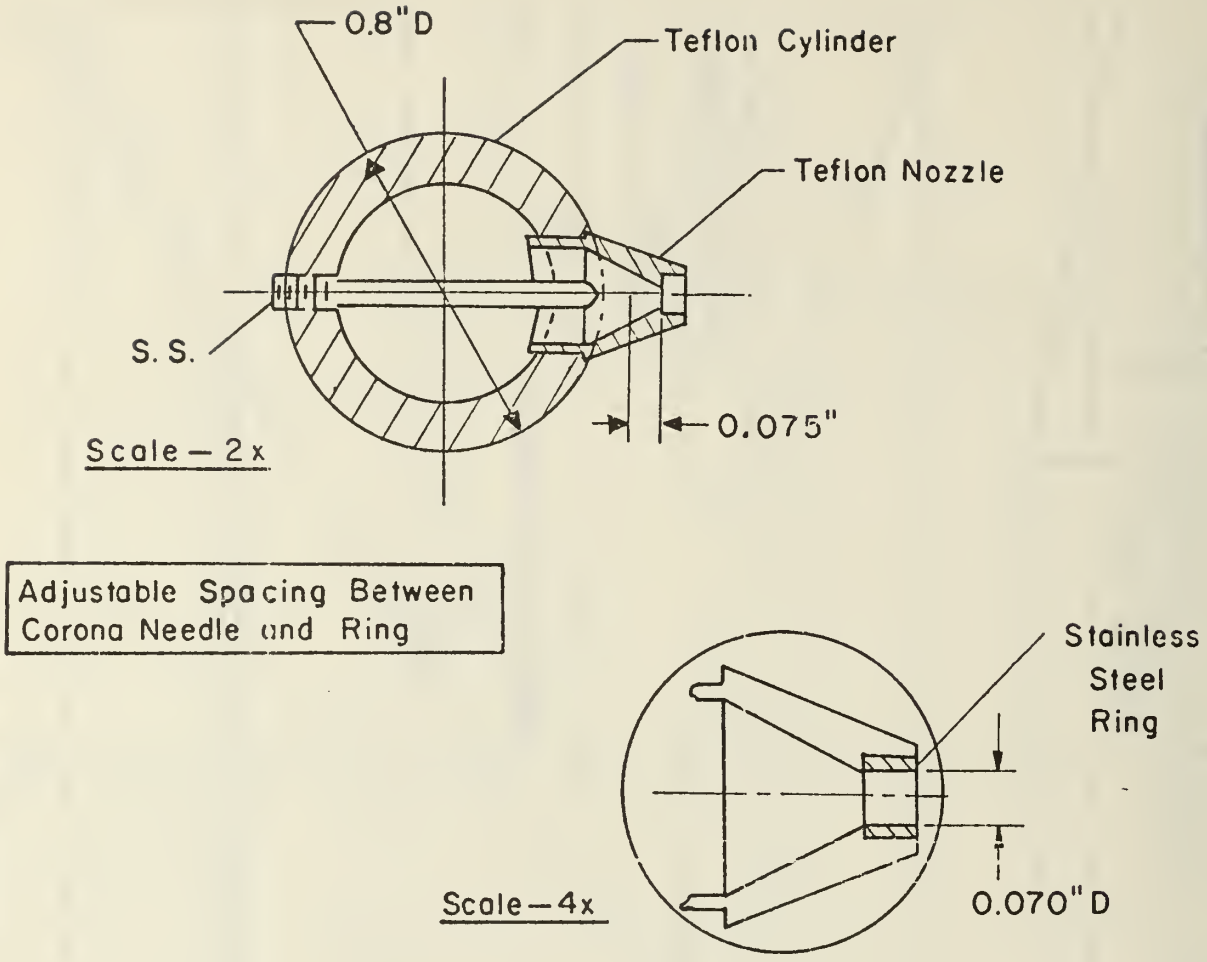

FIGURE 3. AEROSOL INJECTOR

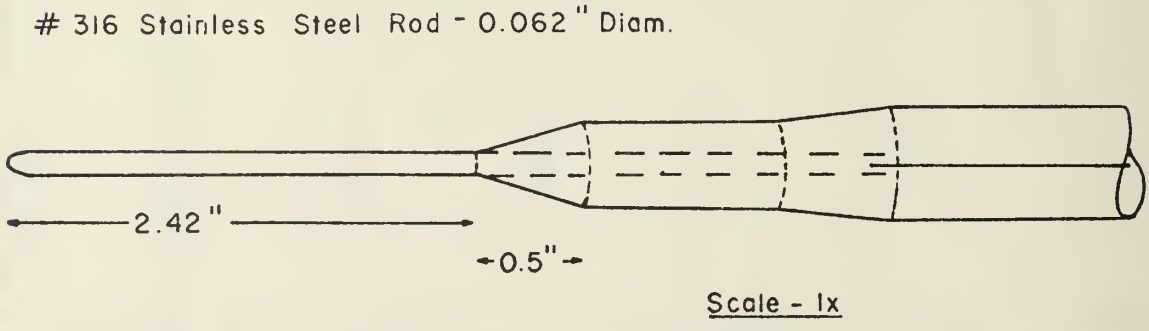

FIGURE 4.
COLLECTOR PROBE

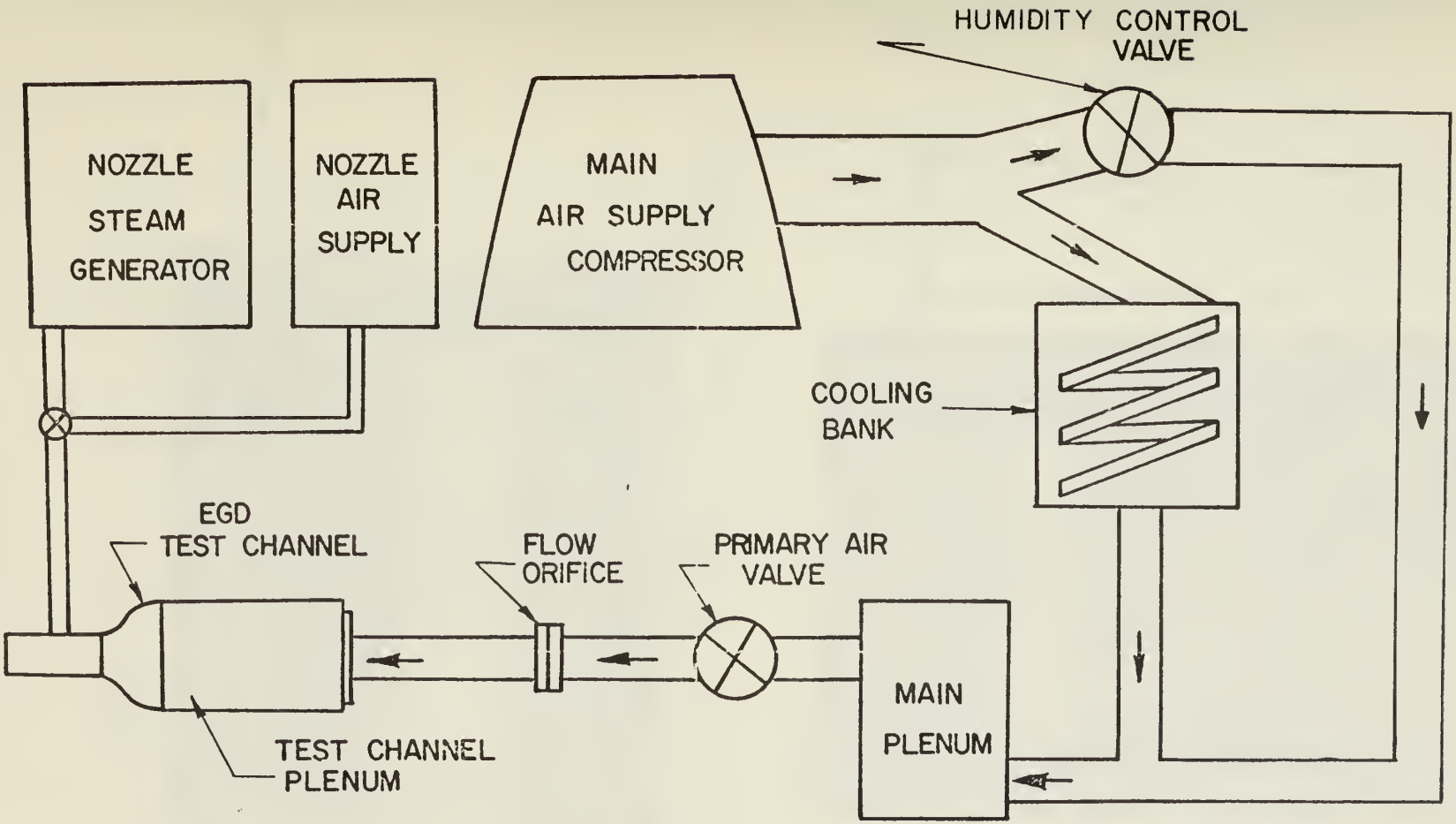

FIGURE 5.

AIR AND STEAM FLOW SCHEMATIC.

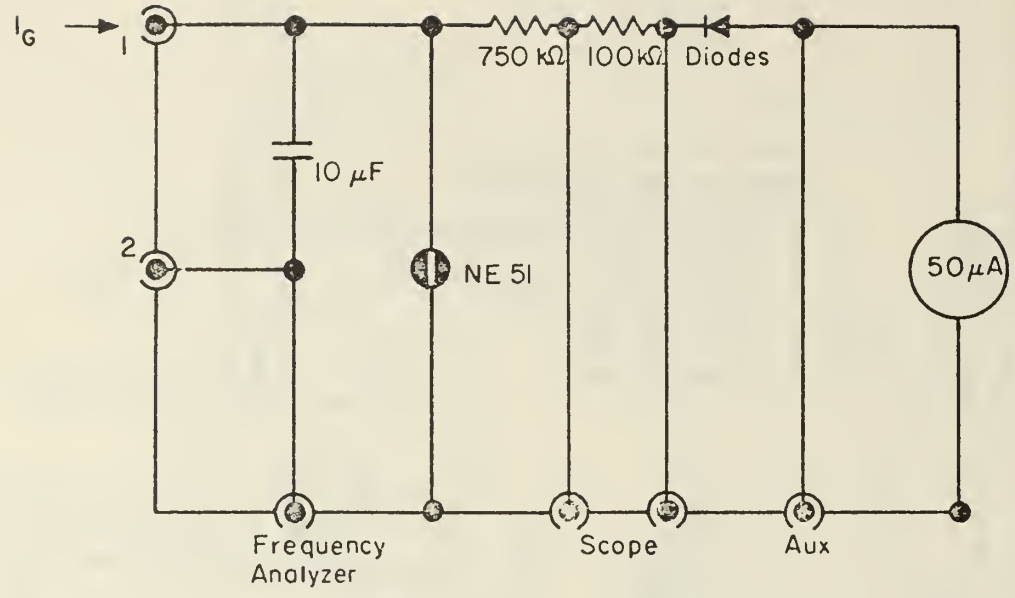

FIGURE 6.
ELECTRICAL SCHEMATIC OF COLLECTOR

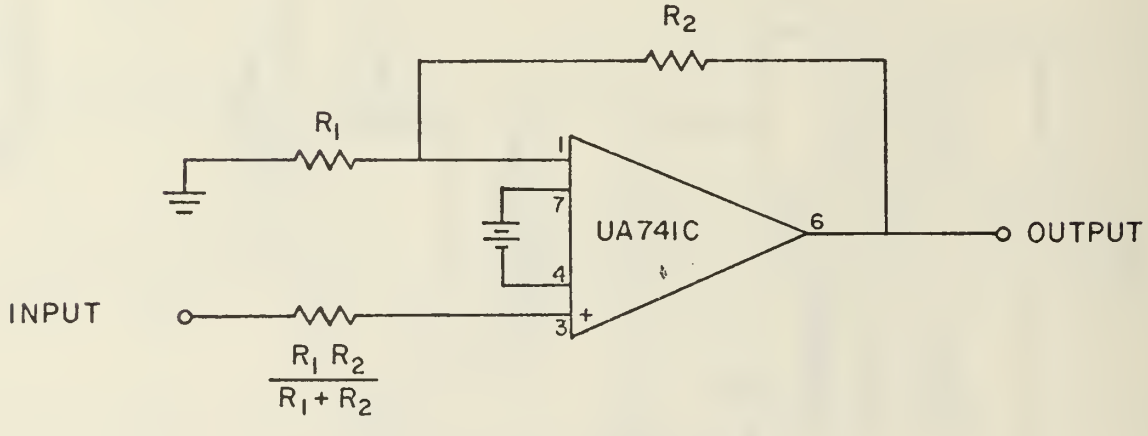

FIGURE 7.
SCHEMATIC OF PREAMPLIFIER

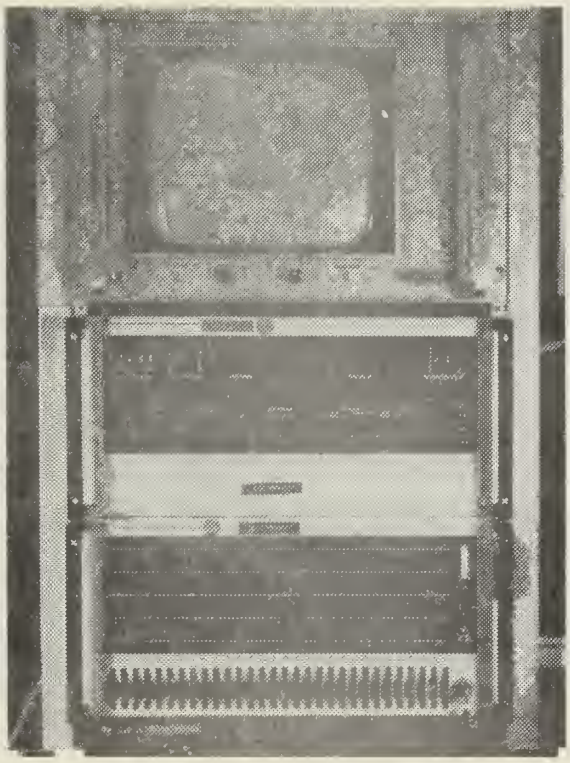

X-Y DISPLAY, RMS DETECTOR AND MULTIFILTER

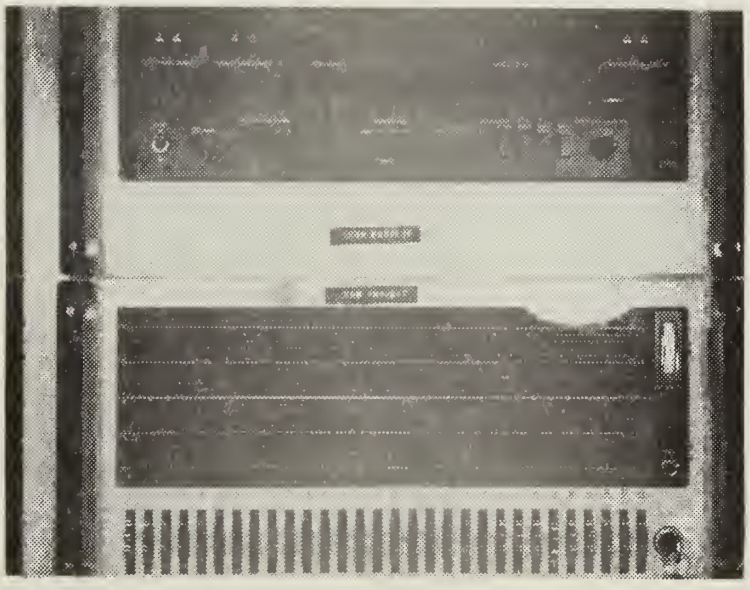

MULTIFILTER UNIT

FIGURE 8
FREQUENCY ANALYZER

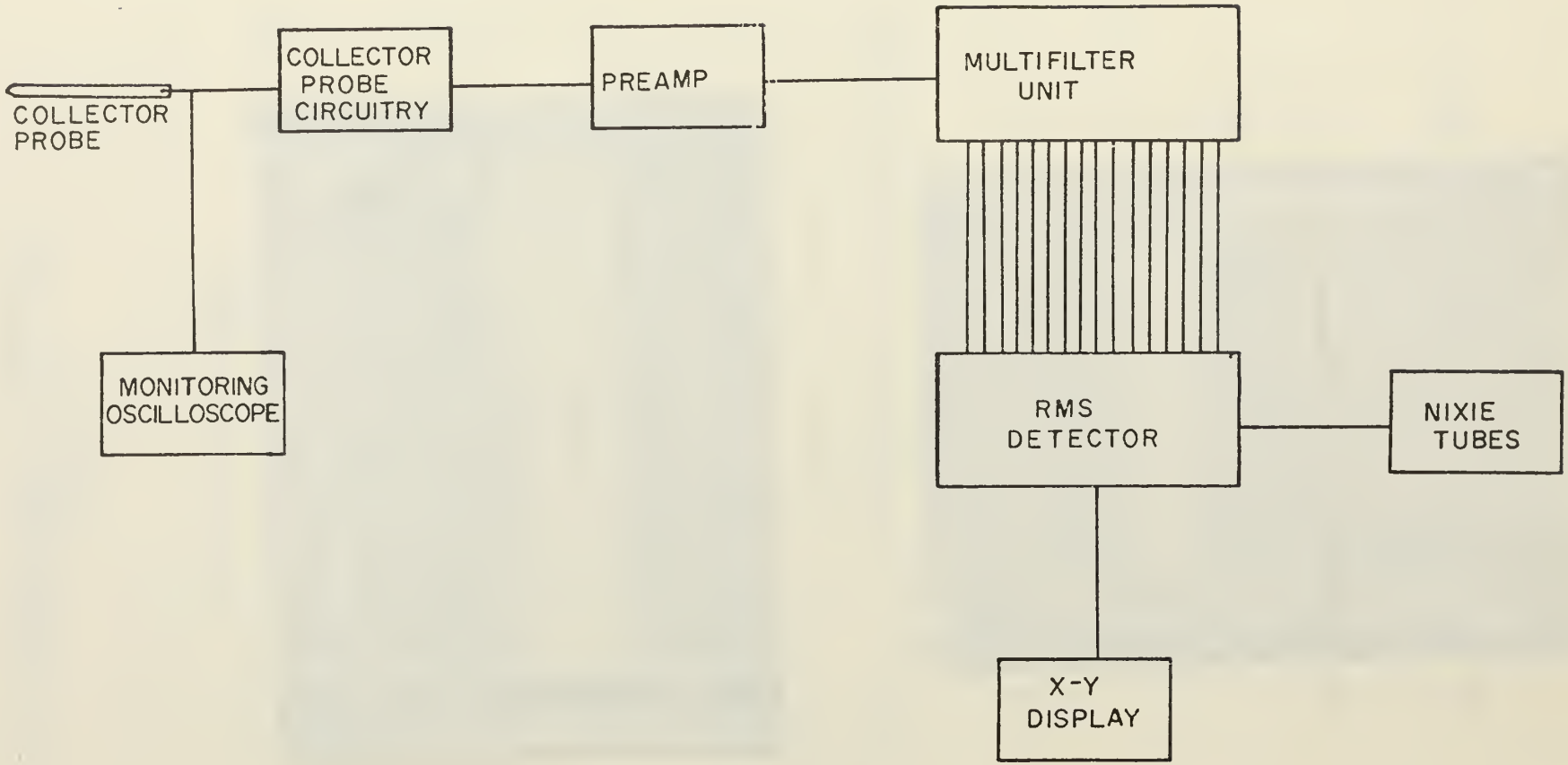

FIGURE 9.
BLOCK DIAGRAM OF SIGNAL FLOW

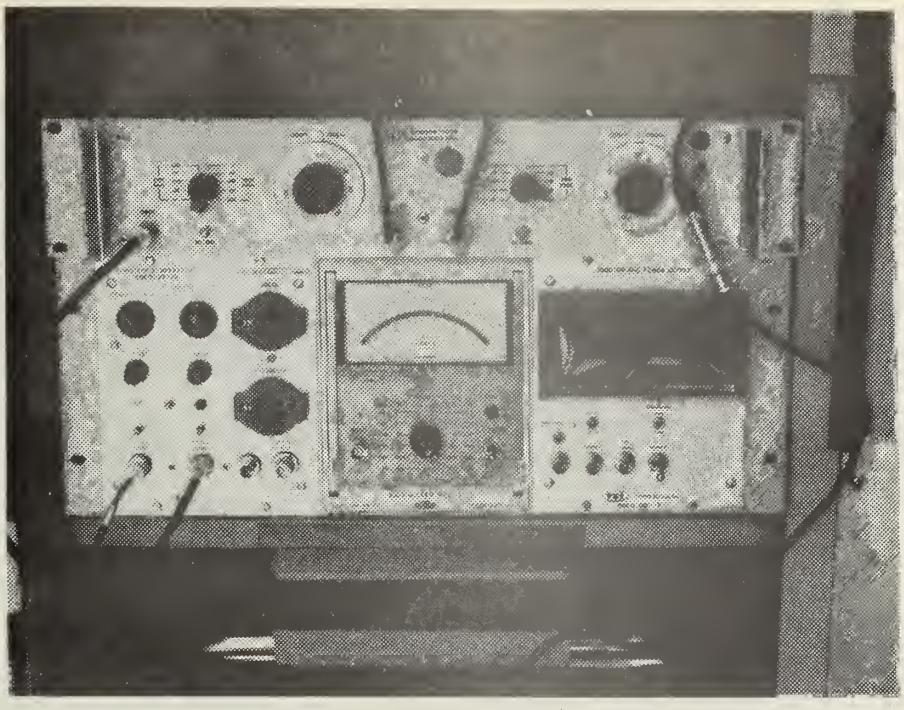

TSI HOT-WIRE ANEMOMETER AND FILTER

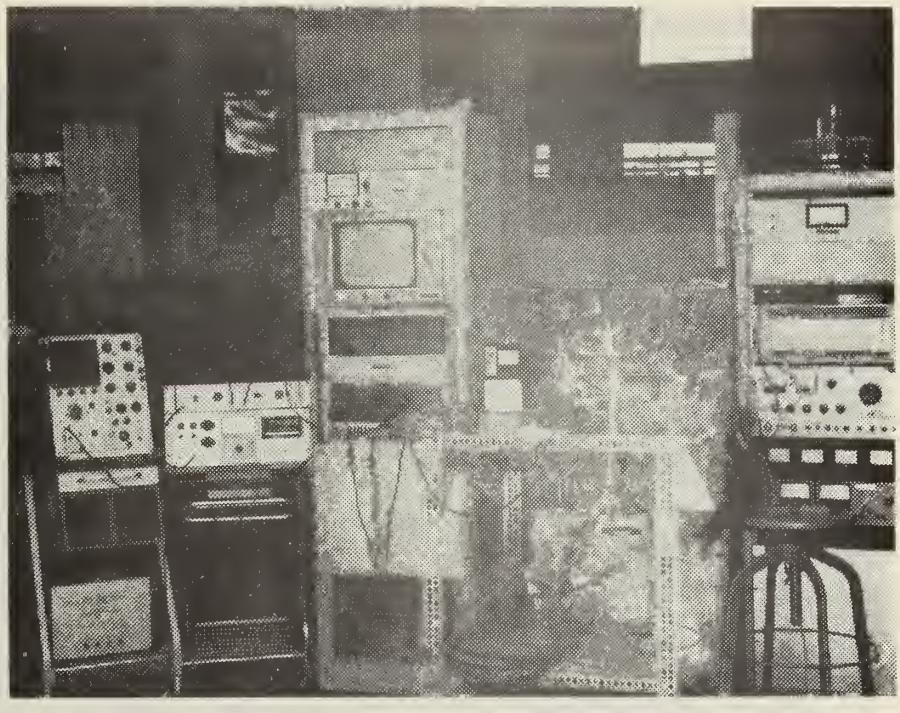

Apparatus Ready for Testing

FIGURE 10
CONFIGURATION FOR HOT-WIRE TESTING

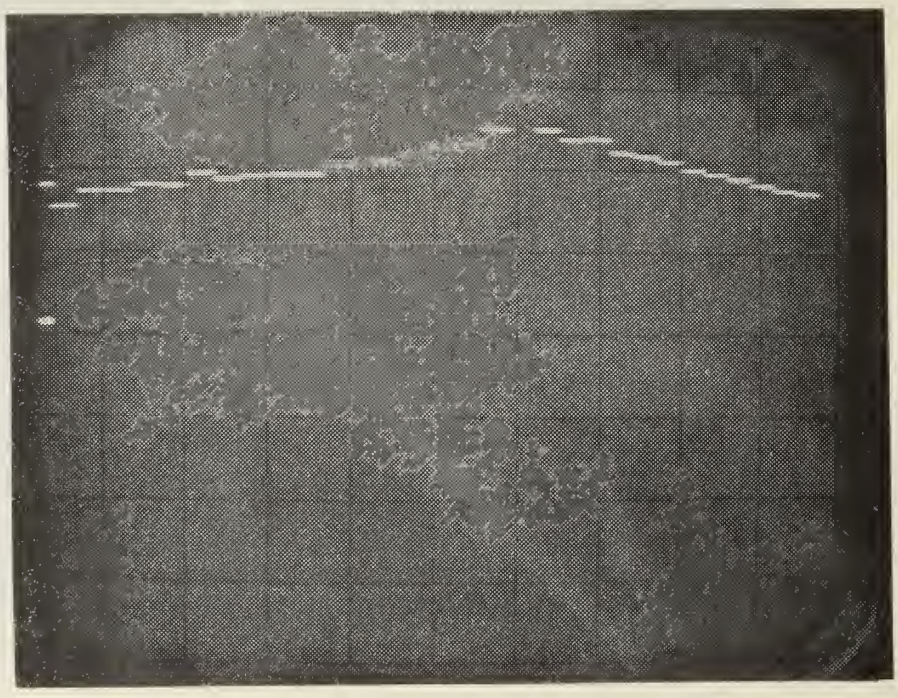

MAIN AIR ONLY (185 fps)

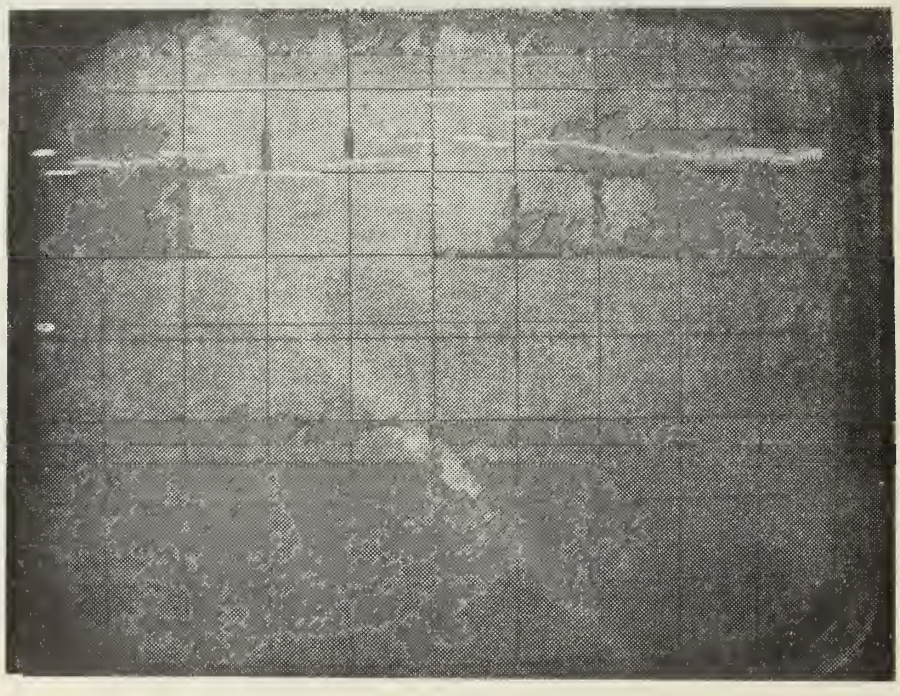

MAIN AIR (185 fps) NOZZLE AIR (8 psig)

FIGURE 11. X-Y DISPLAY FROM HOT-WIRE ANEMOMETER
L = 10 mm (℄)

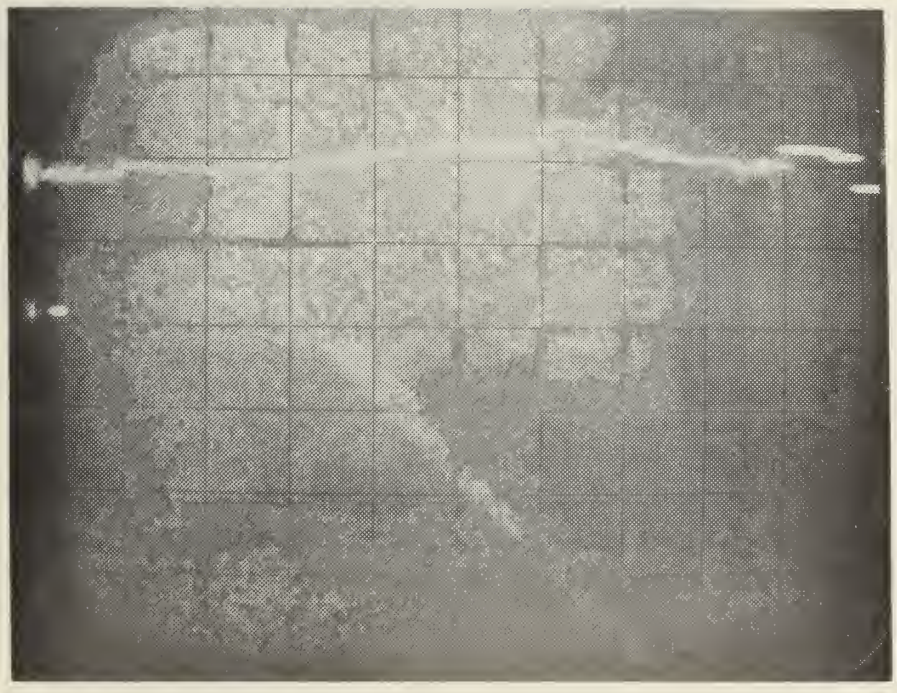

MAIN AIR ONLY (185 fps)

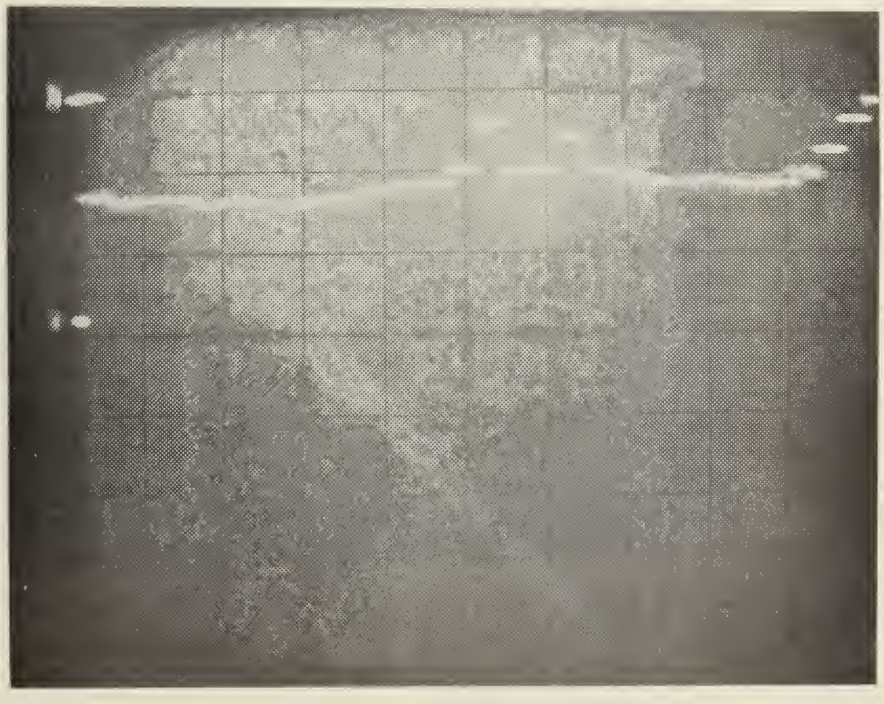

MAIN AIR (185 fps) NOZZLE AIR (8 psig)

FIGURE 12. X-Y DISPLAY FROM HOT-WIRE ANEMOMETER
L = 5 mm (℄)

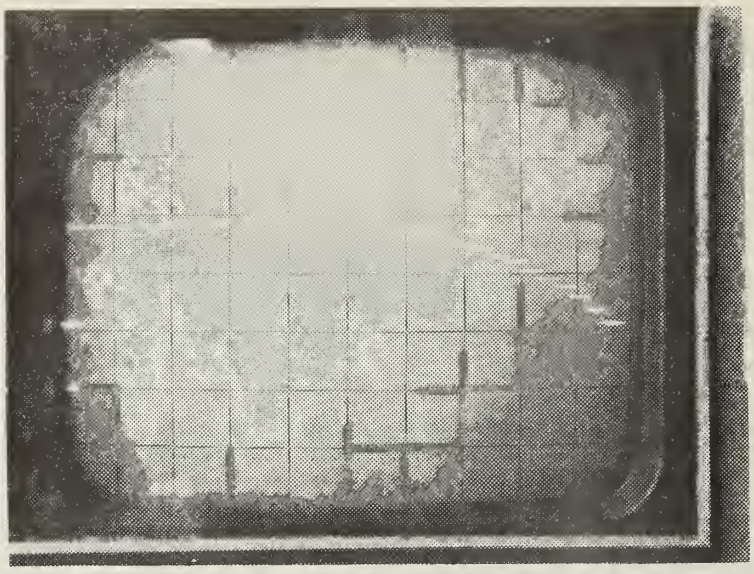

I_G = 0.9 μA, MAIN AIR (185 fps), STEAM (8.0 psig, 245 °F)

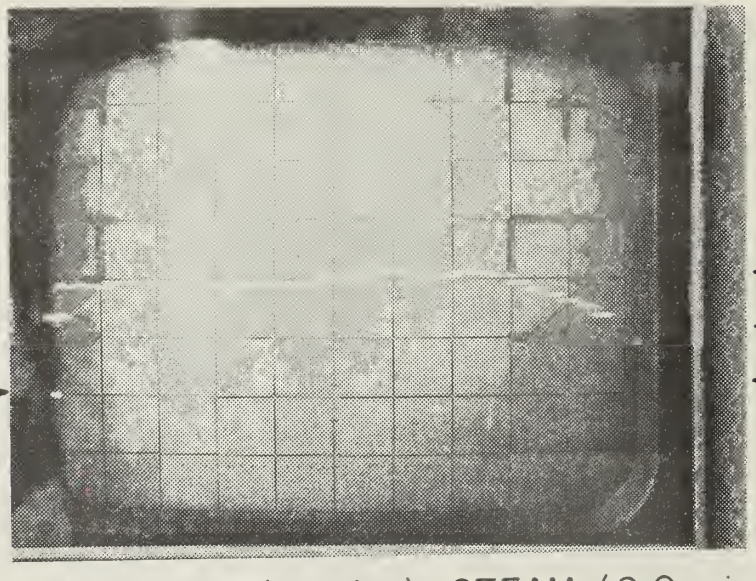

I_G = 0.9 μA, MAIN AIR (185 fps), STEAM (8.0 psig, 231 °F)

FIGURE 13. X-Y DISPLAY FROM EGD PROBE
L = 5 mm (℄)

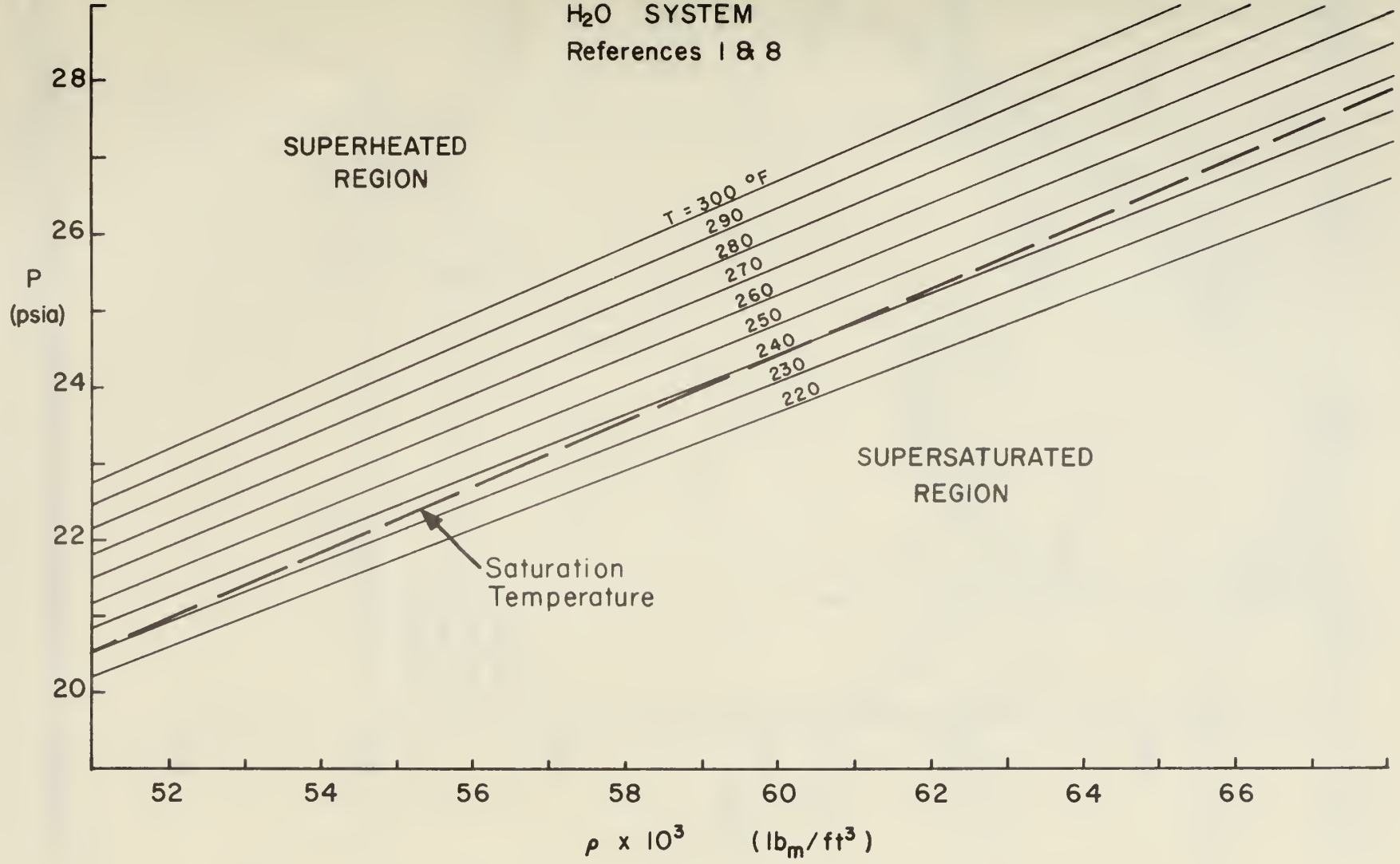

FIGURE 14. PRESSURE-DENSITY-TEMPERATURE PLOT

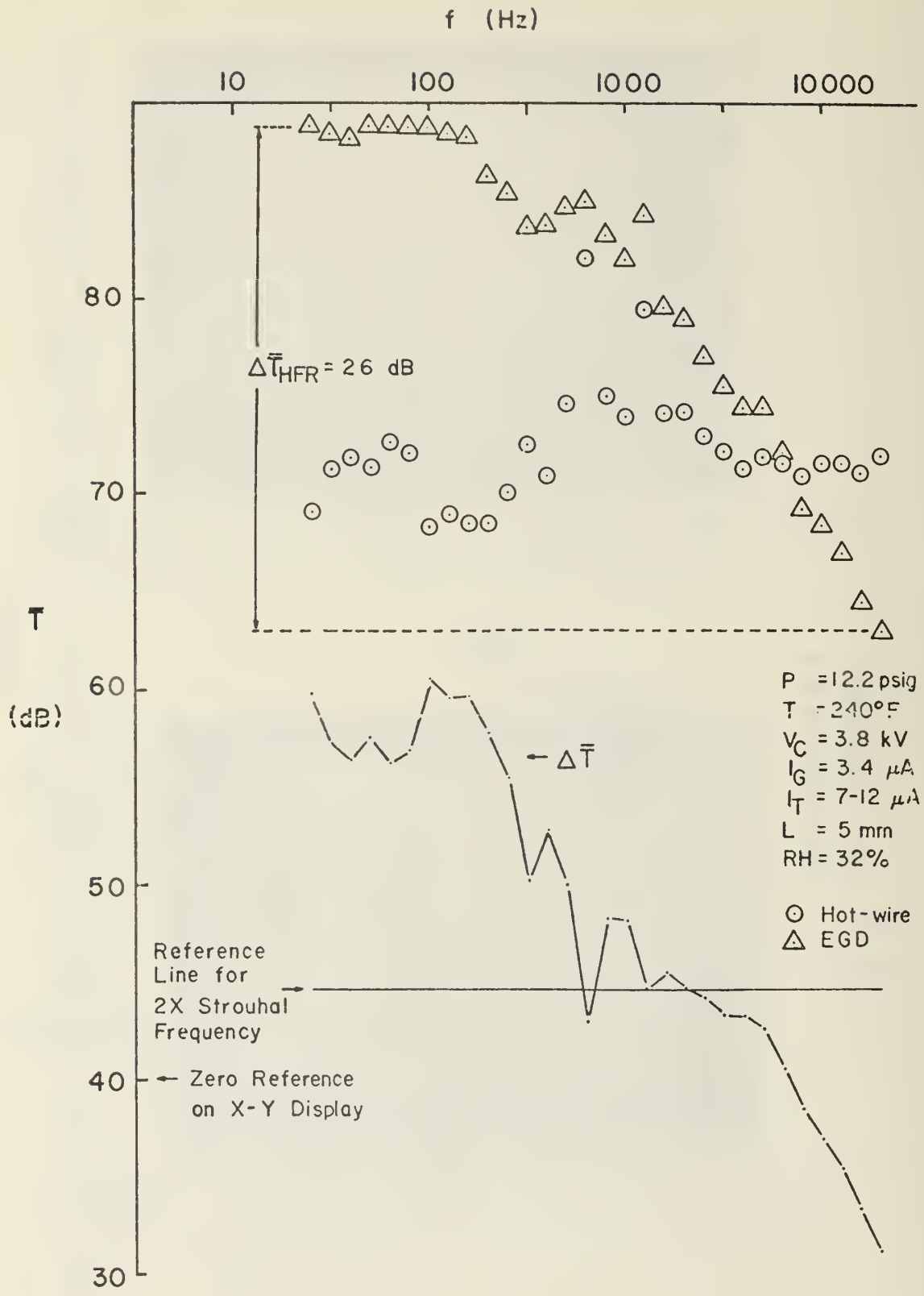

FIGURE 15. COMPARISON OF EGD AND HOT-WIRE DATA

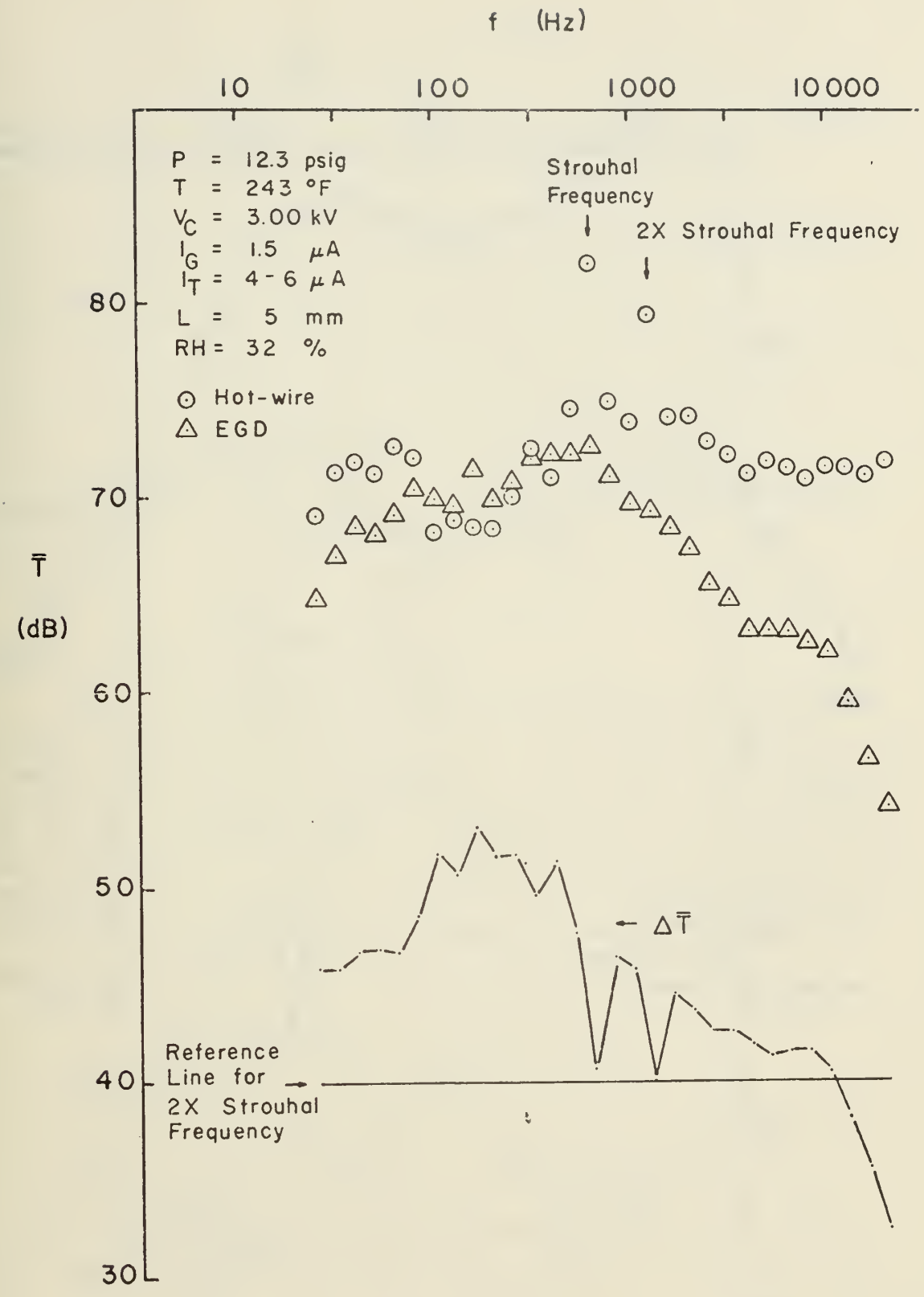

FIGURE 16. COMPARISON OF EGD AND HOT-WIRE DATA

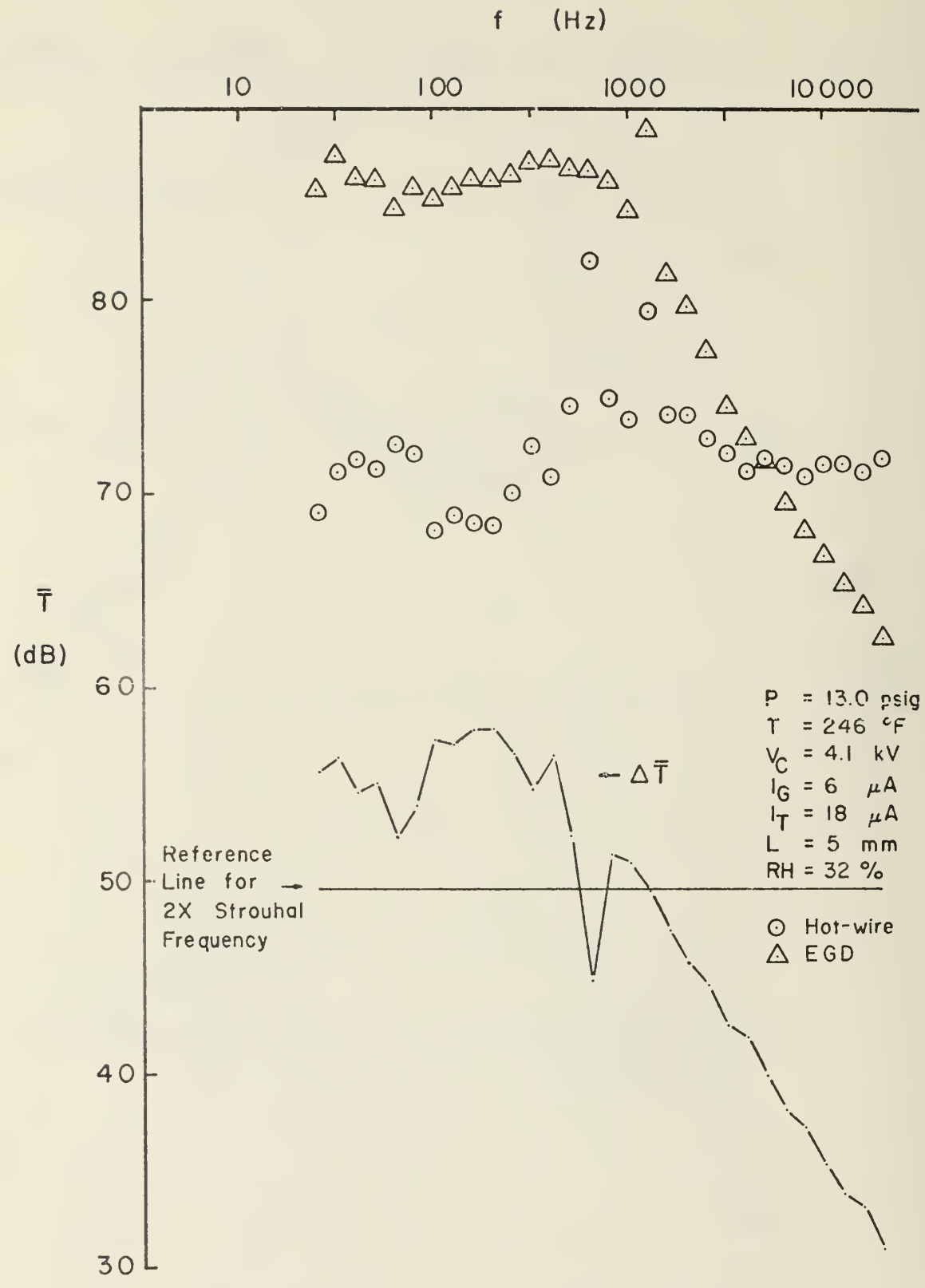

FIGURE 17. COMPARISON OF EGD AND HOT-WIRE DATA

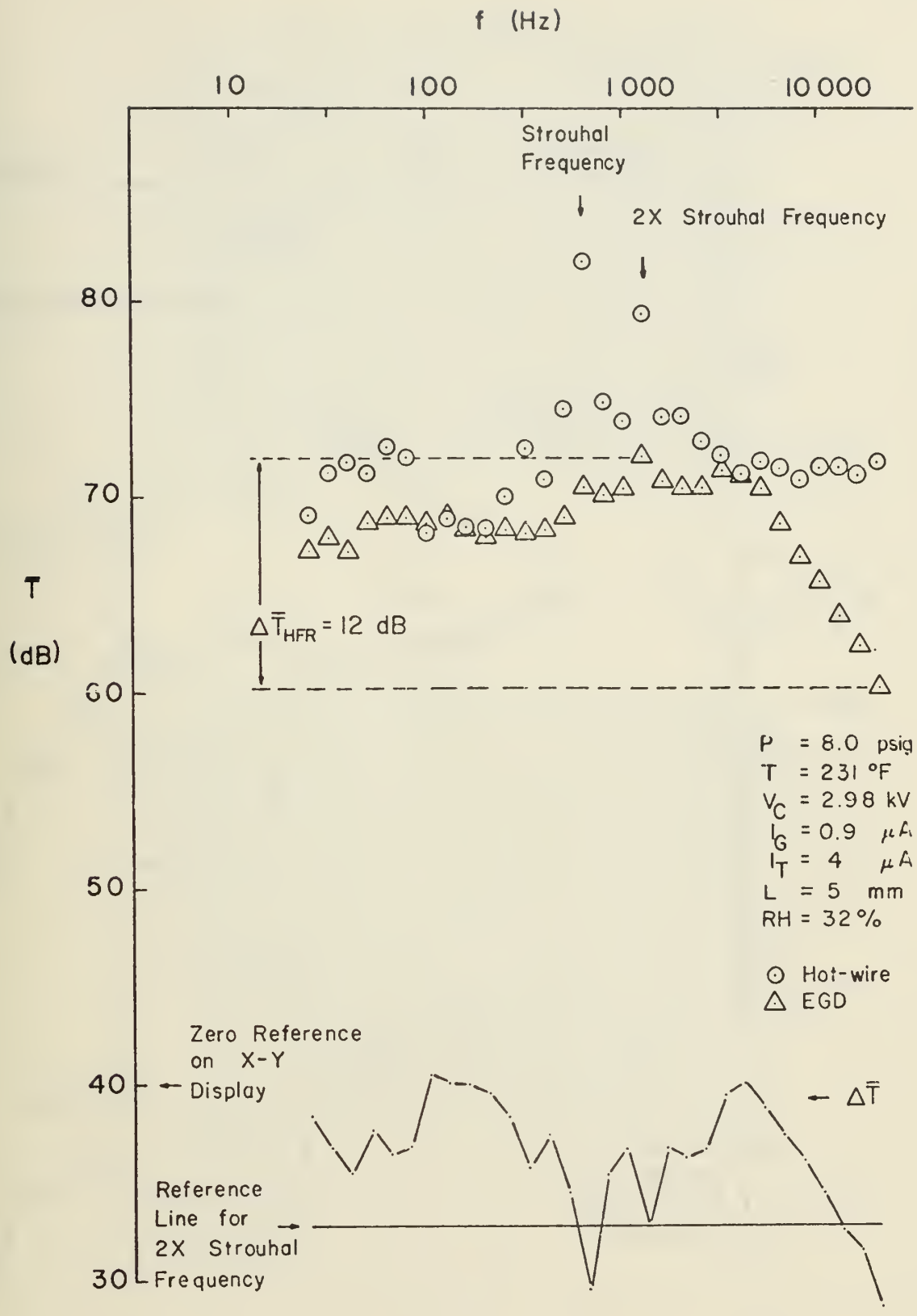

FIGURE 18. COMPARISON OF EGD AND HOT-WIRE DATA

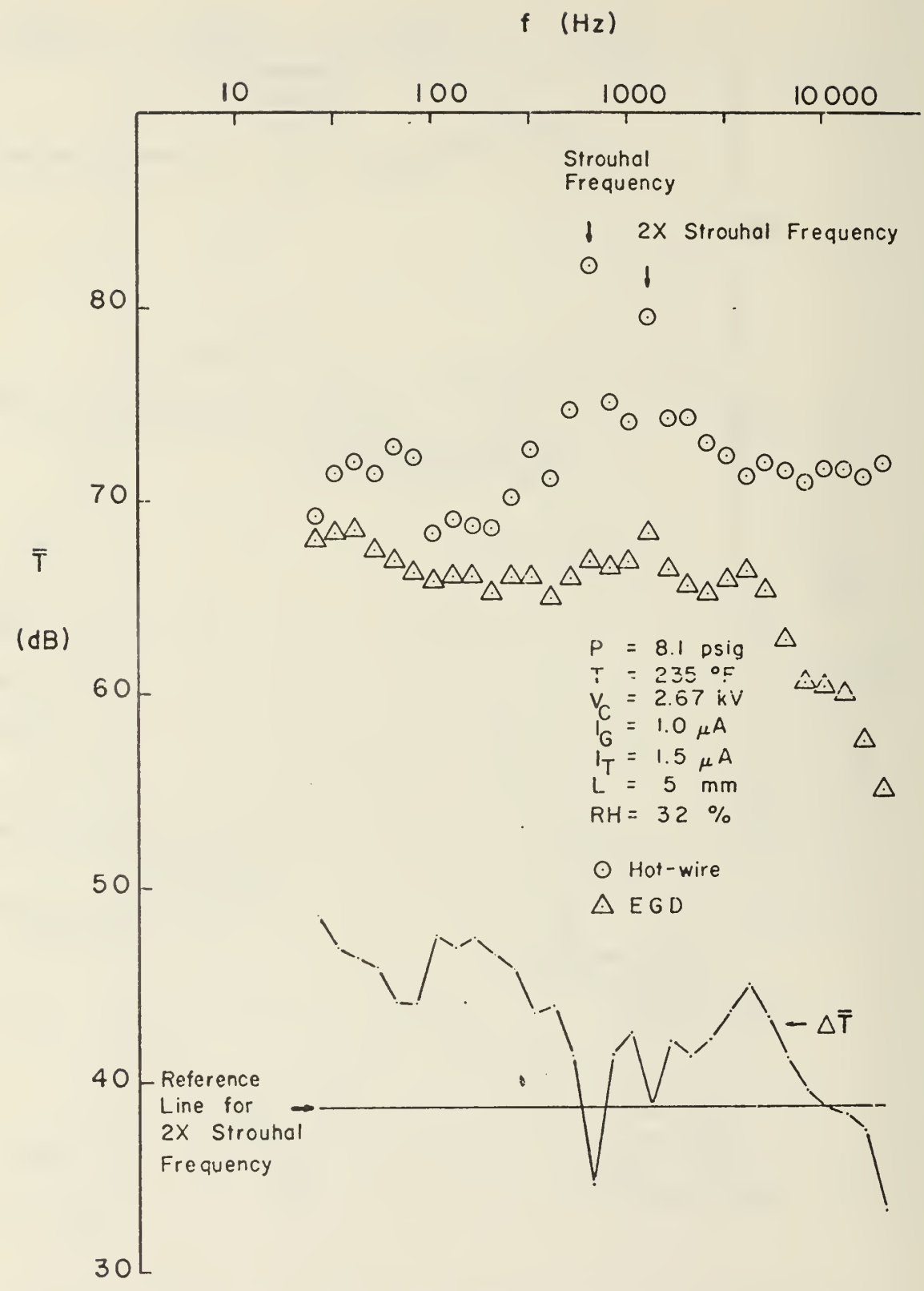

FIGURE 19. COMPARISON OF EGD AND HOT-WIRE DATA

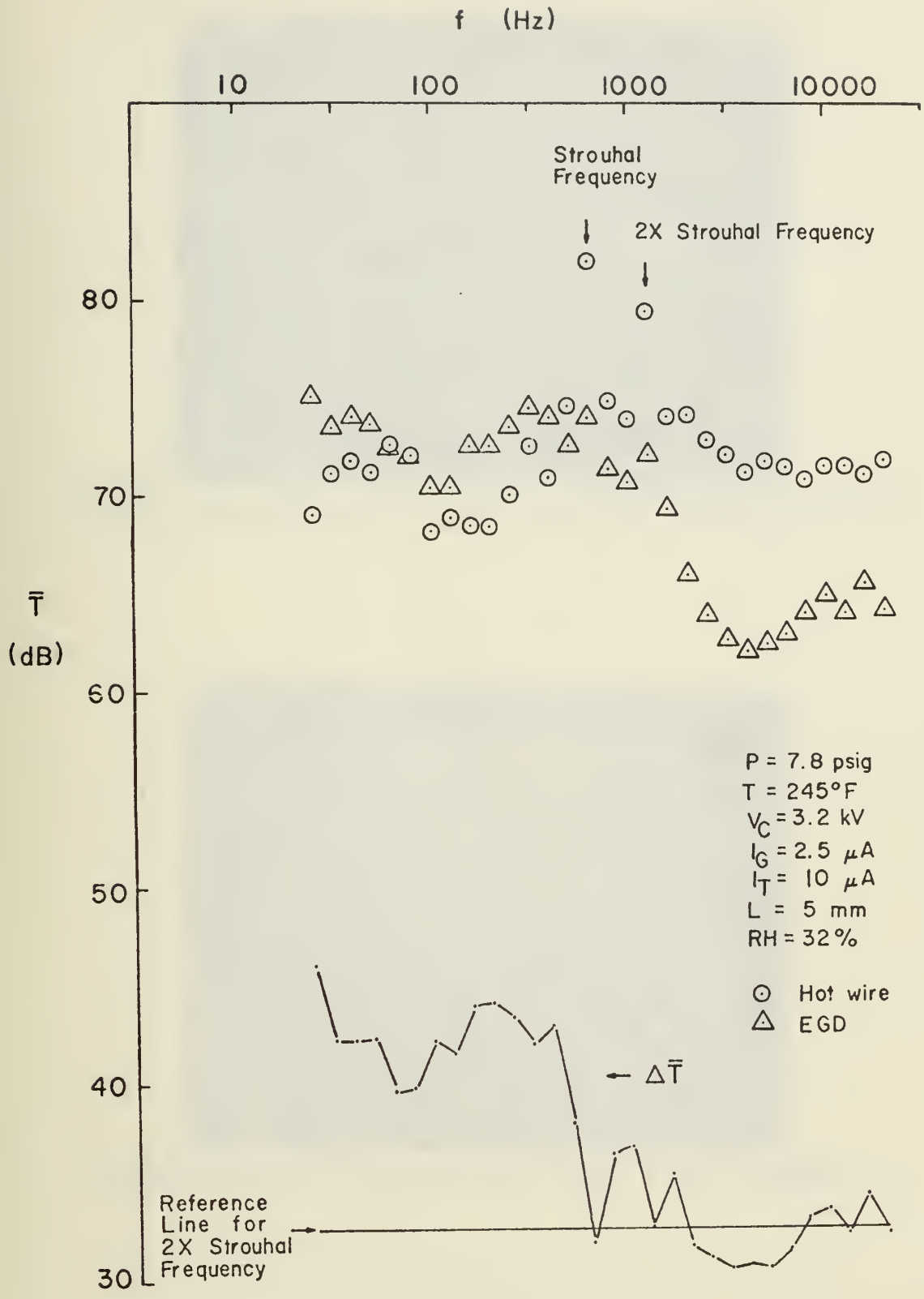

FIGURE 20. COMPARISON OF EGD AND HOT-WIRE DATA

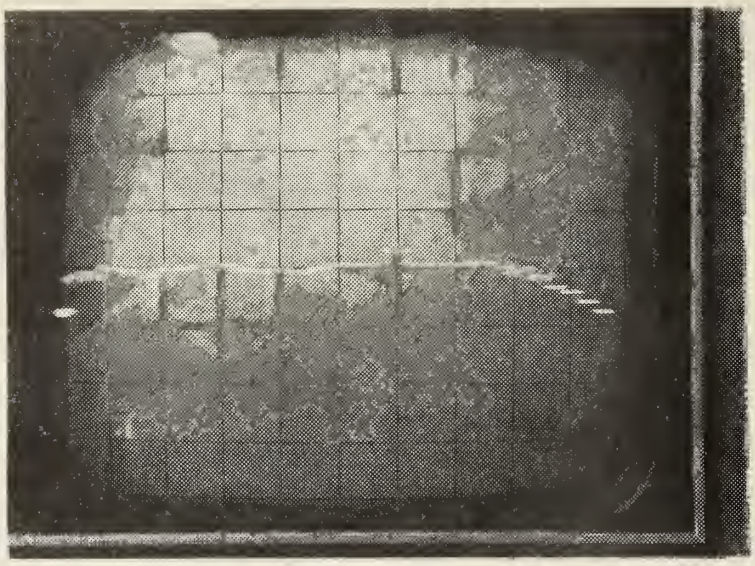

I_G = 1.6 μA, MAIN AIR (185 fps), STEAM (8.0 psig, 230°F)

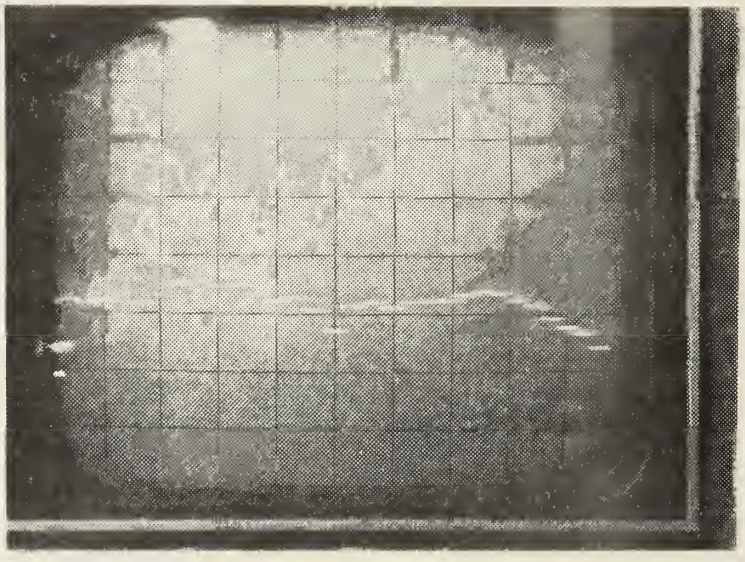

AS ABOVE BUT WITH MULTIFILTER CORRECTIONS

FIGURE 21
COMPARISON OF EGD DISPLAYS

I_G = 0.6 μA, MAIN AIR (185 fps), STEAM (8.0 psig, 230 °F)

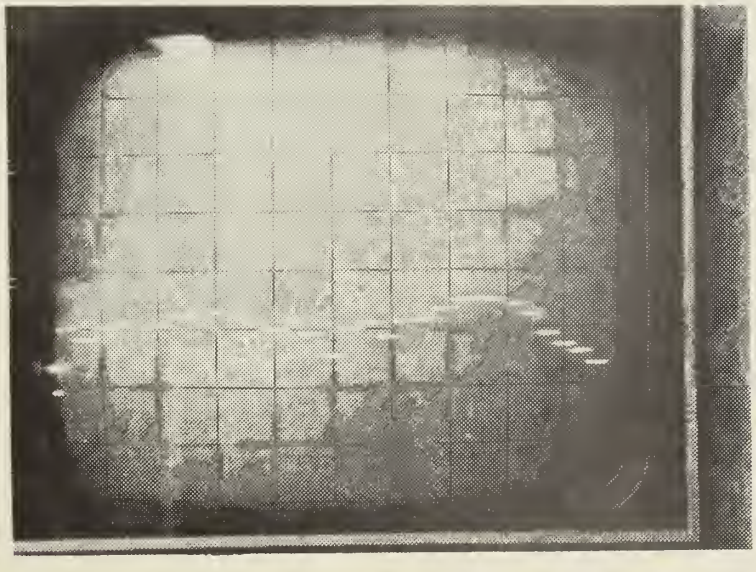

AS ABOVE BUT WITH MULTIFILTER CORRECTION

FIGURE 22
COMPARISON OF EGD DISPLAYS

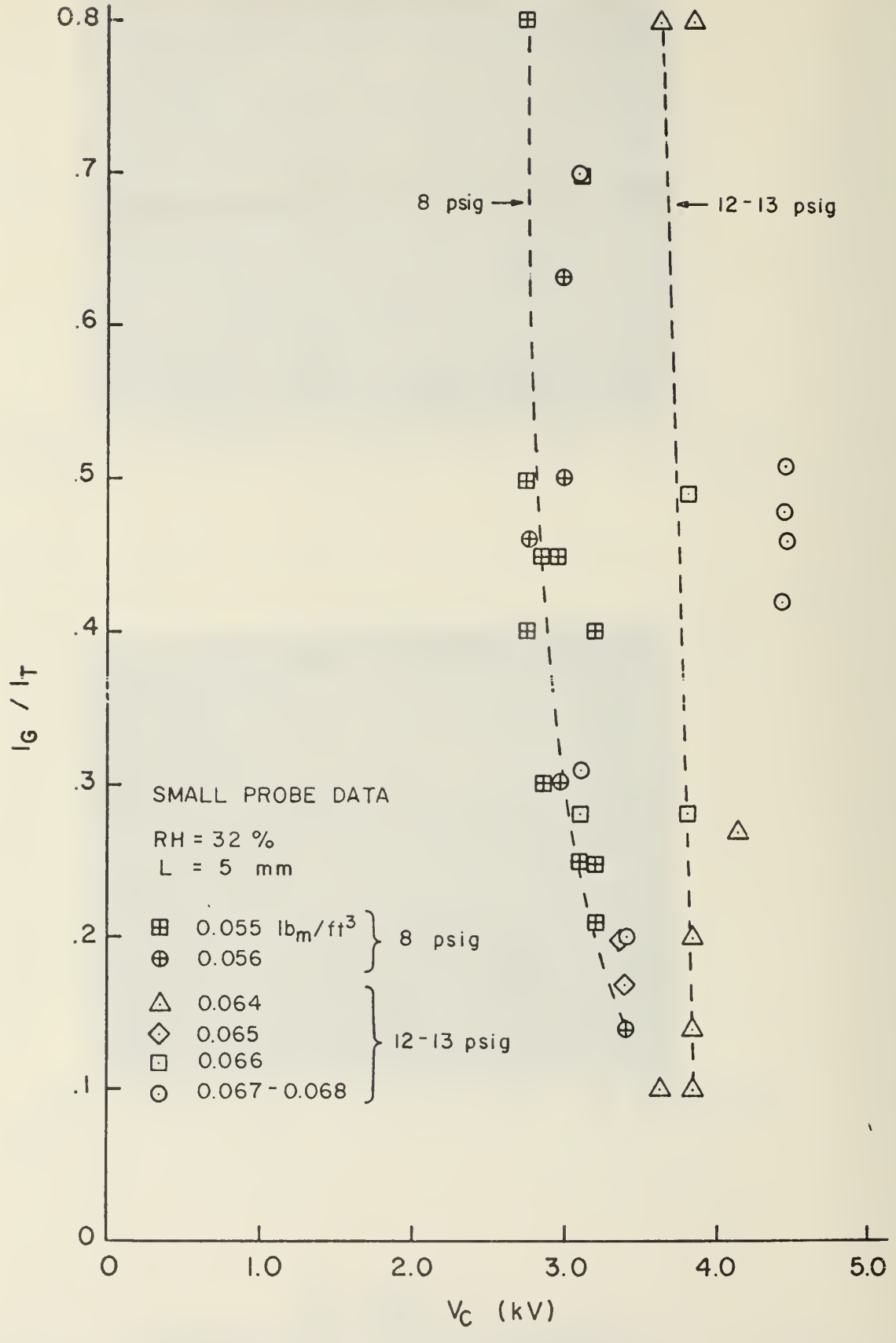

FIGURE 23. EFFECT OF DENSITY ON CURRENT EFFICIENCY

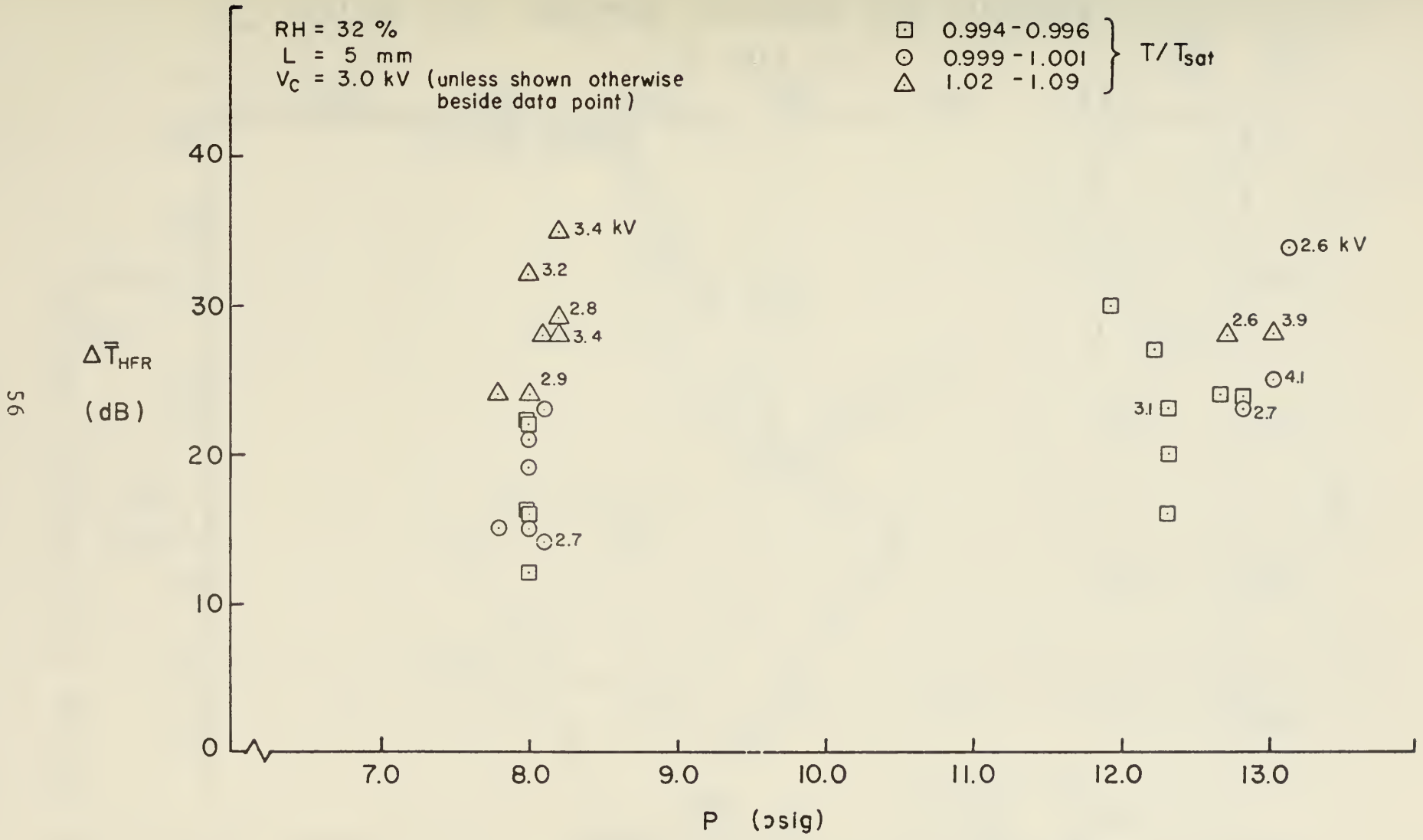

FIGURE 24. OPTIMUM TEMPERATURE AND PRESSURE

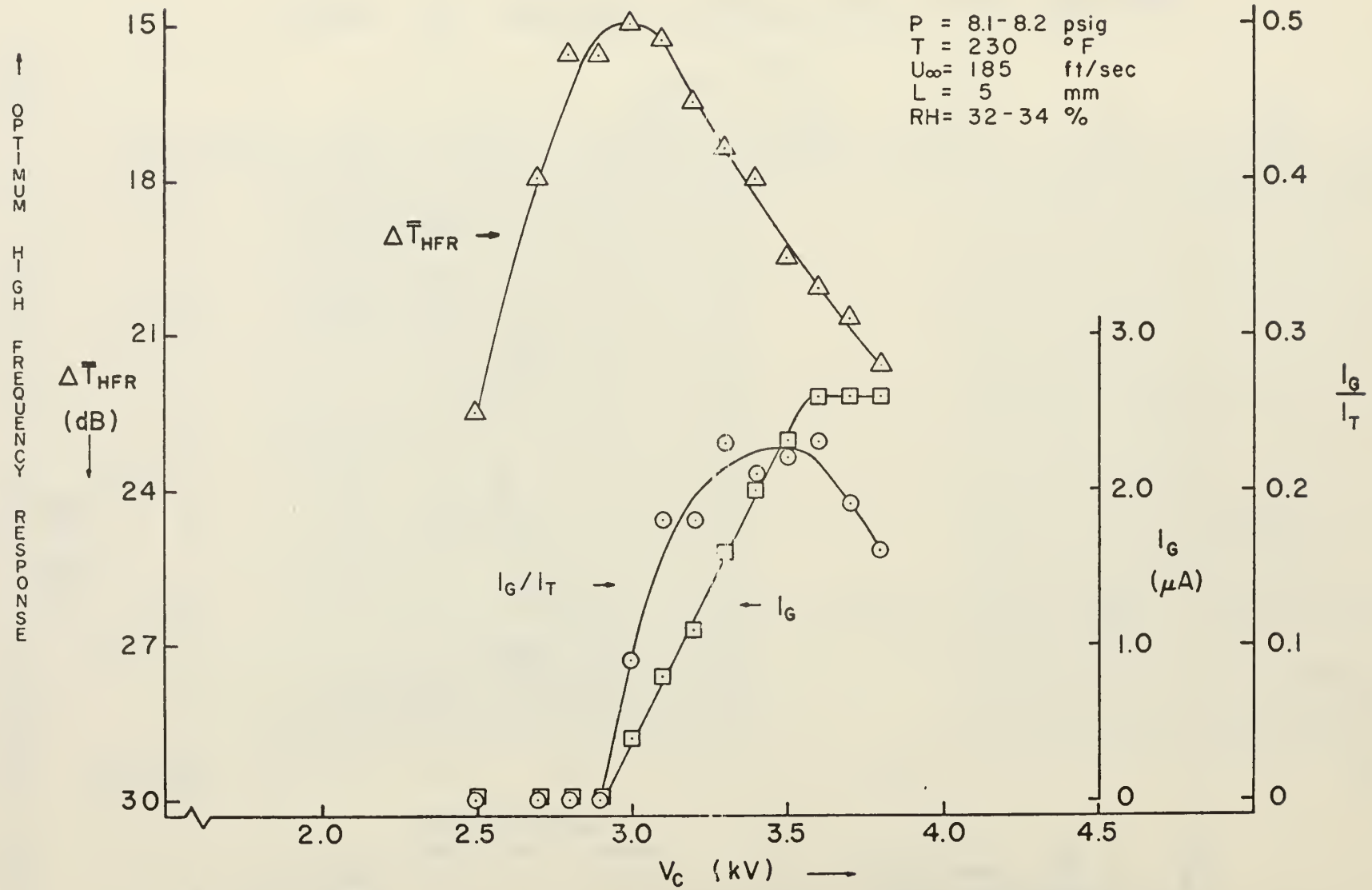

FIGURE 25. OPTIMUM VOLTAGE AND CURRENT

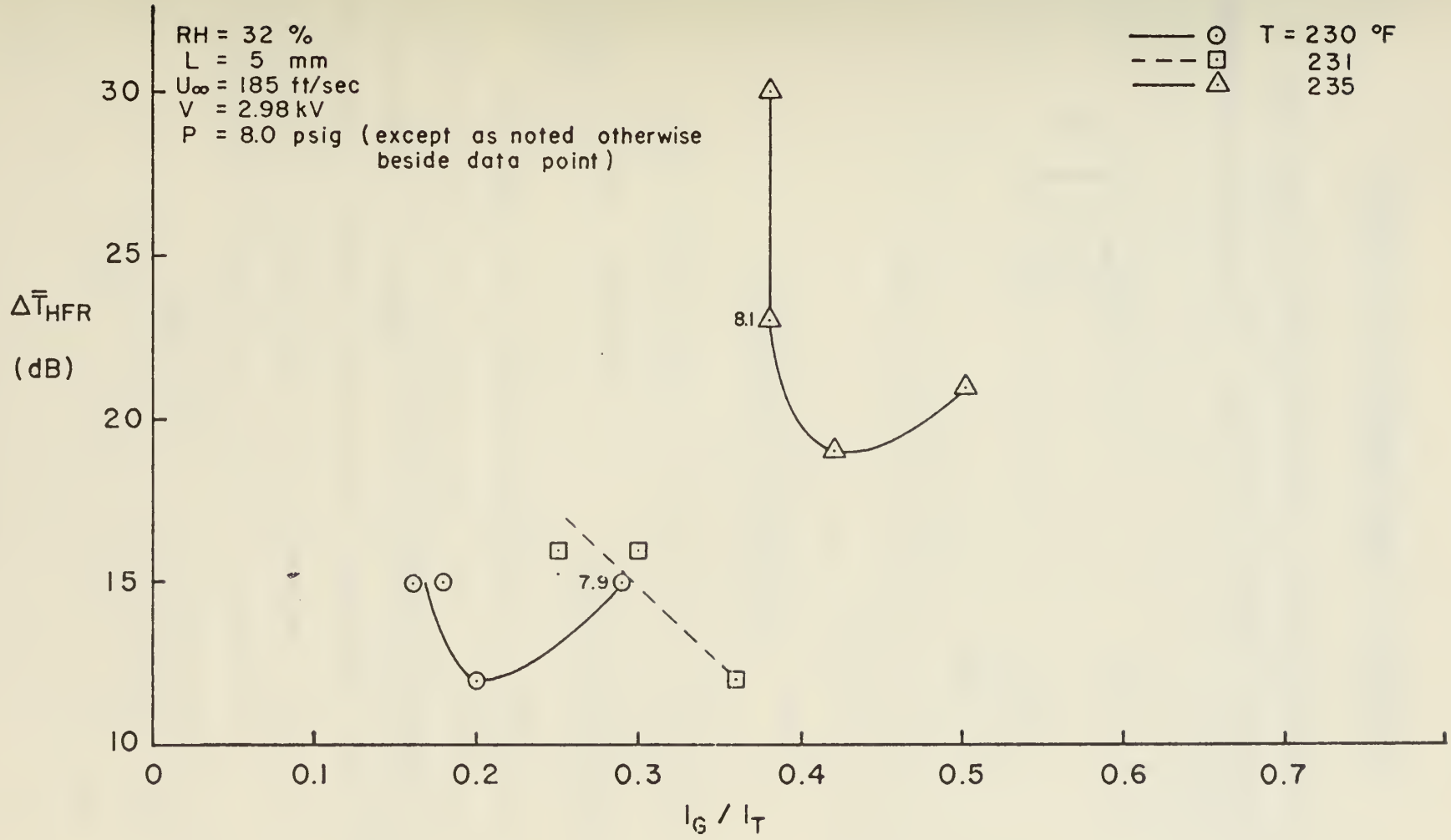

FIGURE 26.
EFFECT OF TEMPERATURE ON HIGH FREQUENCY RESPONSE AS A FUNCTION OF CURRENT EFFICIENCY

APPENDIX A: PHASE SHIFT CALCULATIONS

The phase shift is calculated below in the order in which equipment changes were made. The relation governing phase shift is:

$$\tan \phi = \frac{1/\omega C}{R}$$

$$= \frac{1}{\omega CR}$$

$$= \frac{1}{2\pi fCR}$$

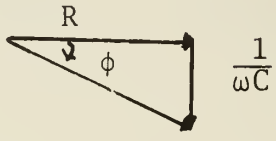

1. C = 0.5 microfarads, R = 100,000 ohms.

   At f = 25 Hertz:

$$\phi = \tan^{-1} \frac{1}{2\ (25)(0.5 \times 10^{-6})(10^{5})}$$

$$= \tan^{-1}\ (0.127)$$

$$= 7.3°$$

   At f = 20,000 Hertz:

$$\phi = \tan^{-1}\ (0.00016)$$

$$= 0°$$

2. C = 10 microfarads, R = 100,000 ohms.

   At f = 25 Hertz:

$$\phi = \tan^{-1}\ (0.0064)$$

$$= 0°$$

3. C = 10 microfarads, R = 825,000 ohms.

   At f = 25 Hertz:

$$\phi = 0°$$

APPENDIX B: DETERMINATION OF V_{RMS}

The signals measured in this investigation are expressed in decibels for ease in manipulation. The decibel is simply a ratio of some power level, W, to a reference power level, W_o, and defined as

$$V_{RMS} = 10 \log_{10} \frac{W}{W_o}$$

$$= 10 \log_{10} \frac{V^2/R}{V_o^2/R}$$

$$= 10 \log_{10} (V/V_o)^2$$

$$= 20 \log_{10} (V/V_o) \text{ dB.}$$

A zero dB gain implies that $V = V_o$. If $V = 10V_o$ then $V_{RMS} = 20$ dB. Likewise, if $V = 100{,}000V_o$ then $V_{RMS} = 100$ decibels.

The signal into the RMS detector is integrated over a four-second period during which each of thirty discrete frequencies are sampled simultaneously 1024 times in one-third octave bands. The detector measures values of voltage with a one-millivolt reference level. This is converted to decibel form using the equation

$$V_{RMS} = 10 \log_{10} \frac{1}{N} \sum_{i=1}^{N} \left[\frac{V(t_i)}{V_o} \right]^2 \quad \text{dB}$$

where

$V(t_i)$ = measured value

V_o = reference level

N = number of samples (binary number).

The computed data are then displayed digitally on the nixie tubes and are projected on the X-Y display in analog form.

A scale-factor adder adjusts the output-level readings. Normally a one-volt RMS input produces an output-level reading of 60 dB. This reading is adjustable in one dB steps to a maximum of 159 dB. This adjustment does not affect the analog output levels.

Thus, in order to determine V_{RMS}, the nixie tubes or the X-Y display are read as follows:

1. Direct Reading from X-Y Display.

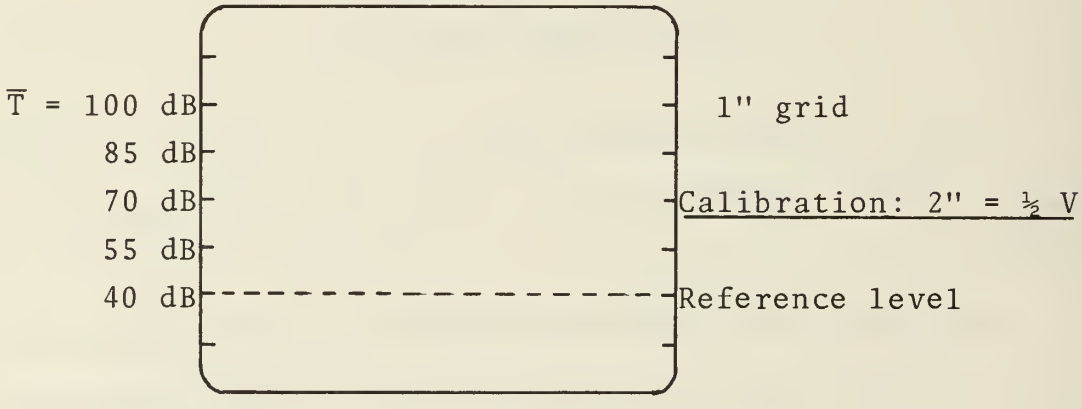

2. Reading from the Nixie Tubes.

X-Y display	Nixie tubes	Remarks
40 dB	40 dB	This reading is present when no signal is injected.
40-80 dB	40-80 dB	Actual values on nixies are correct
80-120 dB	40-80 dB	Add 40 dB to value shown on Nixies to obtain actual value

The frequencies at which measurements are made are displayed both along the x-axis of the X-Y display and on the nixie tubes in the following sequence:

Band	Frequency	Band	Frequency	Band	Frequency
14	25 Hz	24	250 Hz	34	2500 Hz
15	31.5	25	315	35	3150
16	40	26	400	36	4000
17	50	27	500	37	5000
18	63	28	630	38	6300
19	80	29	800	39	8000
20	100	30	1000	40	10000
21	125	31	1250	41	12500
22	160	32	1600	42	16000
23	200	33	2000	43	20000

APPENDIX C: TERMINOLOGY RELATIONSHIPS

From Reference 4, the ratio of the EGD probe output divided by the corresponding $U_{\infty RMS}$, and then normalized, results in

$$T'_g(f) = \frac{I'_g/An_pq}{U_{\infty RMS}}$$

where

I'_g = spectral probe current

A = area of the collector

n_p = number density of charged particles

q = charge per particle

$U_{\infty RMS}$ = RMS value of the fluctuating component of carrier gas velocity.

Let e = reference voltage of one millivolt. Dividing both the numerator and the denominator by e and taking the logarithm of both sides results in

$$\log_{10} T'_g(f) = \underbrace{\log_{10} I'_g/An_pq/e}_{\overline{T}_E} - \underbrace{\log_{10} U_{\infty RMS}/e}_{\overline{T}_h}$$

where now

$\overline{T}_E$ = intensity of the turbulence as measured by the EGD probe and expressed in decibels.

$\overline{T}_h$ = intensity of the turbulence as measured by the hot-wire anemometer and expressed in decibels.

BIBLIOGRAPHY

1. ASME Steam Tables, ASME, New York, 1967.

2. Bennett, W. E., "The Generation of Direct Current at High Potentials," Research Applied in Industry, Vol. 12, No. 12, December 1959, England.

3. Biblarz, O., EHD Research-Final Report for the Year 1968-69, Naval Postgraduate School Report NPS-57ZI9121A, 30 December 1969.

4. Biblarz, O., Woehler, K. E., and Gawain, T. H., EHD Research-Final Report for the Year 1969-70, Naval Postgraduate School Report NPS-57Z10121A, 30 December 1970.

5. Brandmaier, H. E., Dimmock, T. H., and Kahn, B., "Research on Power Generation Electrogasdynamic Energy Conversion," Curtiss-Wright Corp., AR7-67-0008, January 1967.

6. Christianson, R. A., Investigation of the Feasibility of an Electrogasdynamic Probe for Measurements on Mean and RMS Velocities, Masters Thesis, Naval Postgraduate School, Monterey, California, April 1970.

7. Hinze, J. O., Turbulence, McGraw-Hill, 1959.

8. Keenan, J. H., and Keyes, F. G., Thermodynamic Properties of Steam, 1st edition, John Wiley, New York, 1936.

9. Lawson, M. O., and Decaire, J. A., "Investigation on Power Generation Using Electrofluiddynamic Processes," Advances in Energy Conversion Engineering, American Society of Mechanical Engineers, 1967, pp. 473-483.

10. Segen, J. P., Electrogasdynamic Control of Separated Flow-A Feasibility Study, Engineers Thesis, Naval Postgraduate School, Monterey, California, June 1970.

11. Wallace, D. W., Molecular-Ion Electrogasdynamic Flow Channel, Masters Thesis, Naval Postgraduate School, Monterey, California, June 1969.

12. Whitby, K. T., "Generator for Producing High Concentrations of Small Ions," The Review of Scientific Instruments, Vol. 32, No. 12, December 1961.

13. Wilke, T. L., Current Production in a Cylindrical Geometry Electrofluid Dynamic Generator, unpublished, Aerospace Research Laboratories, Wright Patterson AFB, Ohio, July 1970.

DISTRIBUTION LIST

		No. Copies
1.	Defense Documentation Center Cameron Station Alexandria, Virginia 22314	20
2.	Library Naval Postgraduate School Monterey, California 93940	2
3.	Commander Naval Air Systems Command Department of the Navy Attn: Dr. H. R. Rosenwasser, Code AIR-310C	2
4.	Chairman Department of Aeronautics Naval Postgraduate School Monterey, California 93940	1
5.	Professor Oscar Biblarz Department of Aeronautics Naval Postgraduate School Monterey, California 93940	6
6.	Professor J. R. Melcher Dept. of Elec. Engr., Roon 31-141 Mass. Inst. of Technology Cambridge, Massachusetts 02139	1
7.	Professor Albert Solbes Dept. of Aero., Room 37-375 Mass. Inst. of Technology Cambridge, Massachusetts 02139	1
8.	Mr. Alvin M. Marks Marks Polarized Corp. 153-16 10th Avenue Whitestone, New York 11357	1
9.	Dr. M. C. Gourdine Gourdine Systems, Inc. 112 Naylon Avenue Liningston, New Jersey 07039	1

10. Dr. Hans von Ohain — 1
Aerospace Research Laboratory
U. S. Air Force
Wright-Patterson AFB, Ohio 45433

11. Professor A. E. Fuhs — 1
Department of Aeronautics
Naval Postgraduate School
Monterey, California 93940

12. Dr. Ernesto Barreto — 1
Atmospheric Research Center
State University of New York
130 Saratoga Road
Scotia, New York 12302

13. Professor H. R. Velkoff — 1
Dept. of Mech. Engr.
Ohio State University
Columbus, Ohio 43210

14. Dr. Otmar M. Stuetzer — 1
Sandia Corporation
P. O. Box 5800
Alburquerque, New Mexico 87115

15. Dr. Ralph Roberts — 1
Office of Naval Research
Power Program, Code 473
Washington, D. C. 20360

16. Mr. John A. Stakowski — 1
Office of Naval Research
Power Program, Code 473
Washington, D. C. 20360

17. Dr. H. J. Mueller — 1
Naval Air Systems Command
Code AIR 310
Washintgon, D. C.

18. Dr. S. J. Magram — 1
Army Research Office
Arlington, Virginia 22200

19. Air Force Office of Scientific Research — 1
Washington, D. C. 20333
Attn: Power Systems Group

20. Mr. Robert C. Hamilton — 1
Institute of Defense Analysis
400 Army - Navy Drive
Arlington, Virginia 22202

21. Dr. George C. Szego — 1
Institute of Defense Analysis
400 Army - Navy Drive
Arlington, Virginia 22202

22. Mr. S. Cohen — 1
NASA Lewis Research Center
21000 Brookpark Road
Cleveland, Ohio 44135

23. Mr. M. Lawson — 1
Aerospace Research Laboratory
U. S. Air Force
Wright-Patterson AFB, Ohio 45433

24. Dean of Research Administration — 2
Naval Postgraduate School
Monterey, California 93940

25. Professor C. D. Hendricks — 1
Department of Electrical Engineering
University of Illinois
Urbana, Illinois 61801

26. CAPT Amer Chand — 1
Aerospace Research Laboratory
U.S. Air Force
Wright-Patterson AFB, Ohio 45433

UNCLASSIFIED
Security Classification

DOCUMENT CONTROL DATA - R & D

(Security classification of title, body of abstract and indexing annotation must be entered when the overall report is classified)

1. ORIGINATING ACTIVITY *(Corporate author)*
Naval Postgraduate School
Monterey, California 93940

2a. REPORT SECURITY CLASSIFICATION
Unclassified

2b. GROUP

3. REPORT TITLE
EHD Research
Final Report for the Year 1970-71

4. DESCRIPTIVE NOTES *(Type of report and inclusive dates)*

5. AUTHOR(S) *(First name, middle initial, last name)*
Oscar Biblarz

6. REPORT DATE
December 1971

7a. TOTAL NO. OF PAGES

7b. NO. OF REFS
5

8a. CONTRACT OR GRANT NO.
AIR TASK A310310B/551A/2 R02102-001

b. PROJECT NO.

c.

d.

9a. ORIGINATOR'S REPORT NUMBER(S)
NPS-57ZI1121A

9b. OTHER REPORT NO(S) *(Any other numbers that may be assigned this report)*

10. DISTRIBUTION STATEMENT
This document has been approved for public release and sale; its distribution is unlimited

11. SUPPLEMENTARY NOTES

12. SPONSORING MILITARY ACTIVITY
Naval Air Systems Command
Washington, D. C. 20360

13. ABSTRACT

This is the third year-end report on the EHD contract.

Work with the steam injector continued during the past year. The definition of the slip parameter for unsteady flow has been used in conjunction with velocity profiles measured with a hot wire anemometer to evaluate the potential role of EHD (or EGD) in anemometry. A direct measurement of particle size (using holographic interferometry) indicated that there are no particles of size 10^{-4} or greater. A computer program describing the EHD flow has been written.

DD FORM 1 NOV 65 1473 (PAGE 1)
S/N 0101-807-6811

UNCLASSIFIED
Security Classification

A-31408

14 KEY WORDS	LINK A		LINK B		LINK C	
	ROLE	WT	ROLE	WT	ROLE	WT
Electrohydrodynamics						
Electrogasdynamics						
Turbulence						
Anemometry						
Direct Energy Conversion						